Spray-dried Cellulose Nanocrystal Reinforced Polypropylene Composites

by

Xueqi Wang

A thesis submitted to the Graduate Faculty of
Auburn University
in partial fulfillment of the
requirements for the Degree of
Master of Science

Auburn, Alabama
December 9, 2023

Keywords: spray-dried cellulose nanocrystal, polypropylene, maleic anhydride polypropylene, mechanical properties, mechanical interlocking, percolation threshold

Approved by

Yucheng Peng, Chair, Assistant Professor of College of Forestry, Wildlife and Environment
Brian Via, Professor of College of Forestry, Wildlife and Environment
Tom Gallagher, Professor of College of Forestry, Wildlife and Environment
Shaoyang Liu, Associate Professor of Analytical Chemistry, Troy University

Abstract

Cellulose nanocrystal (CNC), a nano-scale structure with unique properties such as high crystallinity, Young's modulus, and strength, is dominantly extracted from lignocellulosic materials and primarily dispersed in aqueous suspension, which cannot meet the requirement of large-scale industrial production of CNC-based composites manufactured by melt compounding process. This research aims to use CNC after spray-drying (SDCNC) to develop high-performance homopolymer polypropylene (HPP) composites with a thermal compounding process. Two specific objectives are to: 1) develop composites with different loading levels of SDCNC particles (5, 10, 15, 20, 30, 40, and 50 wt.%) and characterize the effect of various loadings of SDCNC on composite properties to identify the percolation threshold of SDCNC particles in the matrix and 2) understand the effect of the compatibilizer of maleic anhydride polypropylene (MAPP) at 3, 5 and 7 wt.% on composite mechanical and thermal properties near the SDCNC percolation threshold.

The SDCNC particle reinforced HPP composites (CNC/HPP) with different SDCNC loading levels were prepared through a masterbatch concept. The mechanical behaviors, including tensile, flexural, and impact properties, as well as morphological and thermal properties of the composites, were investigated. Compared to the neat HPP, the tensile and flexural moduli of elasticity (MOE) of the composites significantly increased with increasing SDCNC loading levels. The impact strength of CNC/HPP composites was significantly improved due to the establishment

of mechanical interlocking networks between the SDCNC particles and the HPP matrix. The SDCNC percolation threshold in the HPP matrix was identified between 30 – 40 wt.%. The crystallization behaviors of HPP in the CNC/HPP composites were also changed with the presence of the SDCNC particles due to their nucleation function. The crystallization peak temperatures increased with the increasing loadings of SDCNC particles at 20 and 30 wt.%. They remained constant when the SDCNC particle loading levels (40 and 50 wt.%) were higher than the percolation threshold because the nucleation function of the SDCNC particles saturated at the percolation threshold.

The effect of MAPP on the mechanical and thermal behaviors of the SDCNC particle reinforced HPP composites near the SDCNC percolation threshold was assessed. The introduction of MAPP significantly enhanced the mechanical properties of the composites due to the improved interfacial adhesion between the particles and the matrix. The crystallization behaviors of HPP were also altered in the CNC/MAPP/HPP composites compared to the CNC/HPP composites due to the coverage of the SDCNC particle surface with MAPP through a chemical reaction. In addition, adding MAPP in the composites with an SDCNC loading level higher than the percolation threshold may change the dispersion and distribution of the particles in the matrix.

Acknowledgments

I would like to express my immense gratitude to all the individuals who have helped complete my project and thesis. First, I am sincerely thankful to my advisor, Dr. Yucheng Peng, for his all help throughout the entire program. His extensive professional knowledge, patient guidance, unwavering support, and continuous encouragement motivate me to continue my academic journey. Additionally, thanks to my committee members, Dr. Brian Via, Dr. Tom Gallagher, and Dr. Shaoyang Liu, who have offered valuable feedback and advice regarding improving the project.

I also want to extend my appreciation to Dr. Pixiang Wang, Mr. Justin Crouse, and Dr. Douglas J. Gardner for providing experimental assistance, which is essential to obtain meaningful results. Thank you to my labmate, Ke Zhan, for his sincere help, shared knowledge, and exchanged ideas. I learned more knowledge from our discussion. And especial thanks to all my friends for their friendship, positivity, and belief in my abilities. I am truly grateful for their company and support.

I would also like to thank my parents and husband for their immense love, support, and encouragement during the two years. Their presence in my life gives me more strength to move forward.

Last but not least, I would like to acknowledge the funding support from the Downed Timber Research program funded by USDA Forest Service Southern Research Station and the United States Endowment for Forestry and Communities. Additional support from the Alabama Agricultural Experiment Station and the Hatch program of the USDA National Institute of Food and Agriculture [Hatch project 1023887] is also appreciated. I also thank ExxonMobil Chemical Company for donating polypropylene for this research.

Table of Contents

List of Tables

List of Figures

Chapter 1 Introduction

1.1 Cellulose Nanocrystals

Cellulose, one of the basic structural components in wood, is the most abundant natural polymer with about 10^{10}-10^{11} tons of total annual production. [1] It is the main component in the wood and plants' cell wall and provides their strength and rigidity. The chemical structure of cellulose is shown in Figure 1-1A. It has a long linear chain structure comprised of D-anhydroglucopyranose units (AGU), which are covalently linked to each other by β-1,4-glycosidic bonds. [2] The degree of polymerization (DP) of cellulose (the number of repeating cellobiose units in the molecular chain) is usually used to represent the chain length, which is different in the range from several hundred to many thousands for various species and different treatments of cellulose materials. [3] In general, the DP can be as high as 10,000 in wood cellulose and 15,000 in native cotton plant cellulose. After acid treatment and hydrolysis processes, the DP value is decreased to several hundred because of the decomposition or degradation of cellulose. [3]

There are three hydroxy (OH) groups per AGU placed at C-2 (secondary), C-3 (secondary), and C-6 (primary) positions. In addition, the order of the reactive ability of the three OH groups in each AGU is C6-OH, C2-OH, C3-OH from strong to weak. [4,5] These abundant OH groups located

on cellulose structural surfaces make cellulose have broad chemical reaction and modification capacities.

(A) (B)

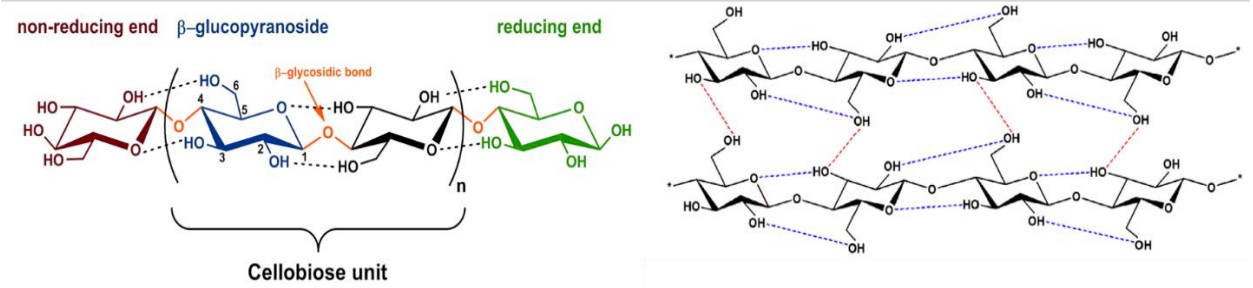

Figure 1-1 (A) Chemical structure of cellulose. [6] (B) Intra- and intermolecular hydrogen bonding networks of cellulose. [6]

As shown in Figure 1-1B, the AGUs in cellulose can form intramolecular hydrogen bonds with the adjacent AGUs in the same molecular chain. Simultaneously, intermolecular hydrogen bonds can also be developed with the neighboring chains, establishing extensive hydrogen bonding networks. [6] The intramolecular hydrogen bonds impart the stiffness of cellulose chain and the intermolecular hydrogen bonds provide the ability for cellulose to form a sheet structure. The linear and organized system of cellulose and the high-density OH groups are responsible for developing the high crystalline structure, which plays an essential role in the mechanical properties of cellulose fiber.

The recent advancement of nanotechnology has developed many novel applications for cellulose nanomaterials – nanocellulose. [7-10] Nanocellulose produced by mechanical or chemical treatments of conventional cellulose fiber is a nature cellulose fiber in nano-scale with at least one

dimension in less than 100 nanometers. [6] Many sources have been explored to manufacture nanocellulose: wood, [11,12] agricultural by-product, [13,14] and animals, [15] bacterial. [16] Nanocellulose has unique properties, such as abundance in nature, biodegradable, high strength, high stiffness, high surface area, etc.. [17,18]

In general, nanocellulose can be classified into three different categories: cellulose nanocrystal (CNC), cellulose nanofibril (CNF), and bacterial cellulose (BC). CNC, also defined as nanocellulose whisker, [19] is a needlelike or rode-like, highly crystalline, short structural material with a typical particle size ranging from about 4-70 nm in diameter and 100-500 nm in length. [20] It is extracted by acid hydrolysis of cellulosic materials. CNF, different from CNC in structure, is a long thread-like bundle of molecules. The diameters of CNF are in the range 3 - 100 nm, but the length is difficult to be determined because of the complex entanglement and the extended network of flexible fibers. [21] CNF consists of crystalline structures and a relatively large portion of amorphous regions when compared with CNC. It is extracted by mechanical disintegration. [24] BC is nearly pure cellulose because of the absence of lignin, hemicellulose, and extractives. It has a finer network structure, resulting in higher mechanical properties than plant-based cellulose fibers. BC can be synthesized into nano-sized fibrils by a genus of bacteria *Gluconacetobacter xylinum* Aceto using glucose as a substrate. [22]

In this project, our research focuses on CNC. CNC is commonly isolated from cellulosic fiber materials by the liberation of crystalline regions when treated by acid hydrolysis. [23,24] Acid penetrates the amorphous regions of cellulose fiber, and chemical reaction begins with the

cleavage of chemical bonds between polysaccharides on the surface of the fibril. The glycosidic bonds that are more easily accessible are hydrolyzed. The amorphous regions are to be removed and disintegrated because they are more readily hydrolyzed under the acid treatment compared with the crystalline regions. Consequently, needlelike cellulose sections with high crystalline structures are generated. [24,25]

CNC is a biodegradable natural material with many unique properties, including nano-scale particle size, low density, high specific surface area, high aspect ratio, outstanding mechanical properties, and numerous surface hydroxyl groups. [26] The excellent mechanical properties, especially the high Young's modulus, attract intensive research effort in developing high-performance composites. [27] The values of Young's modulus of native crystalline cellulose, which have been evaluated both theoretically and experimentally, are in the range of 56-220 GPa with an average of 130 GPa. In addition, the tensile strength of CNC can reach up to 10 GPa. Tashiro and co-workers calculated the three-dimensional elastic constants, Young's modulus, for cellulose crystalline in native form, and the theoretical value along the chain axis was evaluated to 167.5 GPa. [28] Recently, Quesada et al. reported the modulus value is about 200-350 GPa for native cellulose's crystalline section by using a high pressure X-ray diffraction and Raman spectroscopy techniques, respectively. [29] This distinct feature of high stiffness and strength makes CNC an ideal candidate for reinforcing thermoplastic composites.

1.2 The Application of Cellulose Nanocrystal in Thermoplastic Composites

The applications of nanocellulose have been developed in many fields, including polymer composites, [26,30] biomedical utilization for drug delivery and tissues regenerations, [31,32] automotive, [33] food packaging, [34] and wood-based productions. [35] Among these diverse applications, nanocellulose used as a reinforcement in thermoplastic polymer composites has been received considerable attention. Boldizar et al. first reported the utilization of nanocellulose at different loadings as a reinforcing agent for hybrid thermoplastic matrices containing polypropylene, high-density polyethylene and polystyrene. [36] Recently, several reviews have summarized in detail to the application of nanocellulose as reinforcements in polymer composites. [17,23,27,33,37,38]

Herein, CNC used to reinforce thermoplastic polymers will be discussed in depth and in a wide range. CNC possesses higher reinforcing potential compared with other natural and synthetic fillers in reinforced polymer composites. The mechanical properties of different reinforcements commonly used are shown in Table 1-1. [2,39-42] It can be seen that CNC possesses higher tensile strength and Young's modulus than that of conventional natural fibers and some synthetic fillers, such as glass fiber. In addition, Young's modulus of CNC is similar to that of steel wire. However, the CNC is relatively lighter than steel wire based on the comparison of density, which indicates that CNC performs better in lightweight materials as a reinforcing filler.

Table 1-1. Mechanical properties of different reinforcement materials.

Material	Density ($g\ cm^{-3}$)	Tensile strength (MPa)	Young's module (GPa)	Elongation at break (%)
CNC	1.6	7500-7700	110–220	-
Kenaf	1.4	223-930	14.5-53	1.5-2.7
Flax	1.4-1.5	343-2000	27.6-103	1.2-3.3
Jute	1.3-1.5	320-800	8-78	1-1.8
Sisal	1.33-1.5	363-700	9-38	2-7
Cotton	1.5-1.6	287-800	5.5-12.6	3-10
Hemp	1.4-1.5	1270-900	23.5-90	1-3.5
Coir	1.15-1.46	95-230	2.8-6	15-51.5
Bamboo	0.6-1.1	140-800	11-32	2.5-3.7
Kevlar	1.4	3800	124–130	3.6
Steel wire	7.8	4100	210	15
Carbon fiber	1.7	4000	235	1.4-1.8
Glass fiber	2.5	3500	72	2.5-3.4
Carbon nanotubes	1.0	11000-63000	270–950	12

Moreover, CNC also has advantages compared to synthetic fillers regarding environmental benefits. CNC is isolated from abundant renewable sources while synthetic fillers are commonly synthesized from limited abiotic sources. CNC can be biodegraded by organisms while synthetic fillers are persistent and nondegradable. Furthermore, the considerable difference in energy requirement during manufacturing process between CNC (500-2300 $kWht^{-1}$) and other synthetic nanomaterial, e.g., carbon nanotubes (278,000-250,200,000 $kWht^{-1}$) poses an advantageous cost for CNC (1-5 \$ g^{-1}) compared with carbon nanotubes (single wall carbon nanotubes: 80-280 \$ g^{-1}; multi wall carbon nanotubes: 8-15 \$ g^{-1}). [43]

On the other hand, CNC is a high crystalline structure that imparts a good reinforcing ability to the particle. The rigid individual CNC particle with a higher degree of crystallinity, which has a lower amount of amorphous structural defects in the cellulose chain, results in higher thermal stability and greater mechanical strength. [44-46] The reinforcing capability of CNC particle is not only determined by the high crystallinity of the structure, but also by its aspect ratio as shown in Figure 1-2. [47] Bras et al. found a correlation between the stiffness of CNC film and the aspect ratio of CNC and indicated that the tensile modulus of the films increased with increasing aspect ratio of the CNC particles, which was possibly ascribed to the stronger hydrogen bonding interactions between fillers. [48] Besides, CNC with high aspect ratio possesses abundant active hydroxyl groups on its surface. These hydroxyl groups can make CNC high potential to form a rigid percolating network in composites by forming strong interfacial adhesion, such as hydrogen bonds and chemical bonds. The rigid percolating network can further contribute to improve the composites' mechanical properties. [49,50] The formation of the percolation network is usually affected by the homogeneous dispersion of the nanocellulose filler in the matrix. [49,51]

It is worthy of note that a dramatic improvement of the mechanical properties of composites can be achieved by adding a low quantity of CNC particles in thermoplastic matrices. A detailed summary is shown in Table 1-2. Various composites processing methods, including solvent casting and melt compounding, have been employed to prepare CNC-based composites. [52] Melt compounding is environmentally friendly, flexible, cost-effective, and compatible with the industrial process. Because of this, it is broadly accepted in manufacturing thermoplastic

composites. [53-56] The type of thermoplastic polymers that can be utilized as the polymer matrices in CNC-based composites is restricted because the process temperature in the melt compounding process should be controlled under around 260 ℃ where the CNC starts to thermally degrade. [57] PP, with a melting point of 160-166 ℃, is appropriate polymer matrix for developing CNC-based composites fabricated by melt compounding process. It has many benefits, such as light weight with a density of 0.9 g cm^{-3}, good chemical resistance, excellent mechanical and physical properties, and more flexible processing techniques. [58,59] The filled PP composites with the presence of CNC possessed high mechanical properties compared with neat PP (Table 1-2).

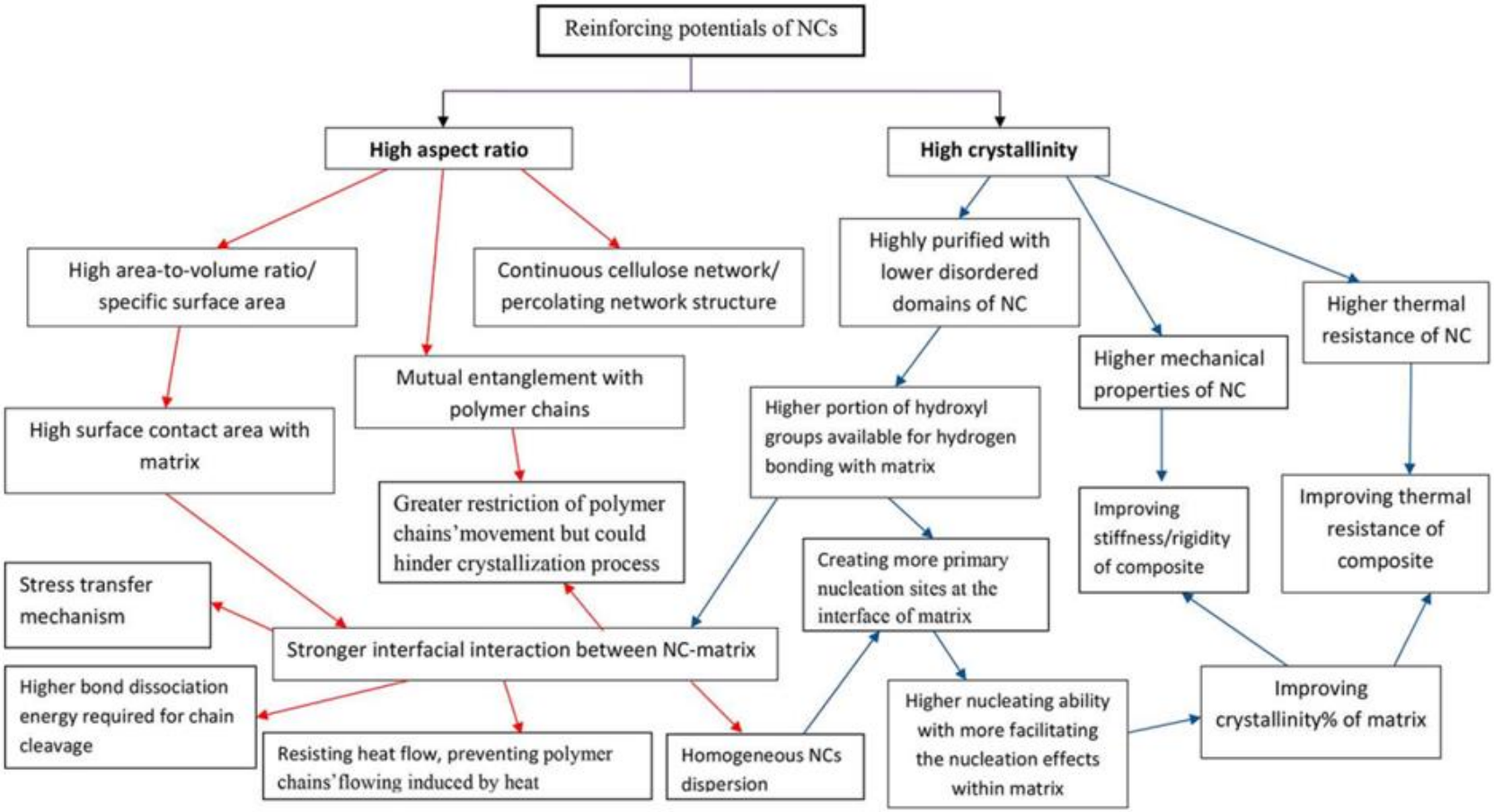

Figure 1-2. Schematic overview of the reinforcing effect of nanocellulose (NC) in polymer systems with different scenarios. [47]

Table 1-2. Mechanical properties of different thermoplastic composites reinforced with CNC.

Matrix	CNC content (wt. %)	CNC source	Tensile strength (%) *	Young's module (%) *	Process	Ref.
PP	5-15	MCC	28-81	(-21)-19	Solution casting	60
PP	5	-	-	60	Melt compounding	53
aPP	6	Tunicin	21-30	1425- 4525	Solution casting	61
PP	2-5	-	7	35	Melt compounding	54
LDPE	5-15	Cotton	23-63	16-33	Solution casting & melt compounding	62
LDPE/TPS	1	-	45	30	Melt compounding	55
PS	1-7	MCC	20-170	-	Electrospinning	63
PLA	1	Cotton	21	27	Solution casting	64
PLA	5	MCC	90	35	Melt compounding	56
PVA	5-15	Wood/cotton	131-174	232-341	Solution casting	65
PVA	15	Ramie	34-82	-	Electrospinning	66
PVA	2-10	Sugarcane bagasse	11.1-17.8	19.4-156.5	Solution casting	67

* % is relative to values of pure polymer samples.

MCC: microcrystalline cellulose; PP: polypropylene; aPP: atactic polypropylene; LDPE: low density polyethylene; TPS: thermoplastic starch; PS: polystyrene; PLA: polylactic acid; PVA: polyvinyl alcohol.

1.3 Problem Statement

Despite the numerous attractive characteristics of CNC there are several limitations when including CNC in an industrial scale composite production process. One challenge is associated with the aqueous suspension format of CNC, which is energy inefficient and cost-prohibitive for a large-scale industrial production. [68] Drying CNC while maintaining the original dimensions for expanding its application on an industrial scale is necessary. Various drying techniques, including oven drying, freeze drying, spray drying, and supercritical drying, have been explored to produce dry CNC. [69]

Peng and co-workers examined these four drying methods and proposed that the spray drying method is most suitable for the generation of dried CNC as fillers in manufacturing composites via melt compounding process. [69] With the current availability of SDCNC in a pilot scale in CelluForce, [70] research on the reinforcing impact of SDCNC in thermoplastic composites is necessary. The morphology of SDCNC particles showed spheric and mushroom cap (or donut) shapes (Figure 1-3). [71] The unique morphology of SDCNC can potentially have a specific impact on composite properties. One assumption we are testing in this proposal is that the mechanical interlocking between SDCNC and thermoplastic can significantly improve the composite mechanical properties. The mushroom cap or donut shape of SDCNC particles has pores on the surface structure (Figure 1-3). The melt polymer matrix can fill these pores. After cooling down, the mechanical interlocking between SDCNC particles and polymer matrix can be established and

help increase the forces needed to separate the interface. Therefore, it is appropriate to hypothesize that the morphology of SDCNC plays a crucial role in reinforcing thermoplastic composites.

Another limitation in the development of SDCNC reinforced polymer composites is the inherent incompatibility between the hydrophilic nature of SDCNC and the hydrophobic thermoplastic polymer matrix. The incompatibility restricts the even dispersion/distribution of SDCNC particles in hydrophobic matrix and results in the weak interfacial adhesion between SDCNC and polymer matrix. The poor dispersion and adhesion have a negative impact on the final composite's properties. [72,73] The poor dispersion is caused by the irreversible agglomeration of cellulose owing to the formation of hydrogen bonds by the interaction between hydroxy groups located on surface. [74] In order to enhance the compatibility between cellulose and hydrophobic polymer matrix, surface modification by physical and chemical methods is generally applied to cellulose. The abundance of hydroxyl groups on the surface of cellulose provides a potential for various chemical modifications, including esterification (reaction with acetic anhydride), etherification (introducing silane coupling agent), oxidation (TEMPO), and grafted polymer of maleic anhydride grafted PP (MAPP). [75] These various surface modification strategies are to decrease cellulose's surface energy which is the main reason for the incompatibility. [47] The lower surface energy of cellulose helps to reduce intermolecular affinity between cellulose particles, decreasing agglomeration. Among these methods, maleic anhydride grafted polyolefin has been proposed to be an efficient way of modifying the cellulose-filled polyolefin composites. [5,57,76-78]

MAPP is the most common compatibilizer in improving the interfacial bonding in cellulose-filled PP composites. [77] Qiu et al. reported a positive effect of MAPP on the interfacial adhesion between cellulose and PP by eliminating the large voids at the interface of cellulose and PP. Meanwhile, adding MAPP to filled composites can increase the tensile strength from 23.7 to 33.7 MPa. [79] Both the thermos-oxidative stability of PP/cellulose composites and the nucleating effect of cellulose fibers for the crystallization of PP were increased with the presence of MAPP. [80]

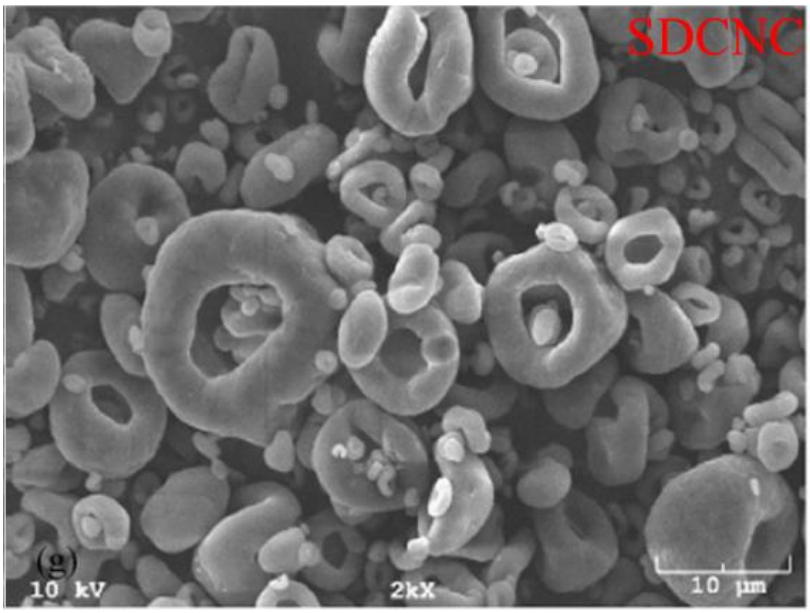

Figure 1-3 The SEM micrograph showing the morphologies of SDCNC (Peng, Han, and Gardner 2012b).

1.4 Objectives and Methodologies

The overall goal of this research is subdivided into two specific objectives: 1) develop composites with different loading levels of SDCNC particles and characterize the effect of loading levels of SDCNC on composite mechanical and thermal properties and then identify the percolation network or distribution of SDCNC particles in HPP matrix and 2) understand the effect of the compatibilizer of maleic anhydride polypropylene (MAPP) on composite mechanical and

thermal properties near the SDCNC percolation. Additionally, the effect of SDCNC percolation on the mechanical and thermal properties of filled HPP composites was investigated.

This thesis consists of two sections presented in the following Chapters 2-3. Chapter 2 mainly concentrates on the fabrication of HPP composites with different SDCNC loading levels (5, 10, 15, and 30 wt. %) using an internal mixer and injection molding equipment. The effect of different loadings of SDCNC on HPP composites mechanical properties, including tensile, flexural, and impact, morphological, and thermal properties was investigated. The water resistance behavior of HPP composites with varying SDCNC concentrations was also studied. Chapter 3 further research on the effect of SDCNC loading levels (20, 30, 40, and 50 wt.%) on HPP composites performance and identify the percolation network or internal structure of SDCNC particles in HPP composites. The impact of SDCNC percolation threshold on the mechanical properties, crystallization and melting behaviors of HPP composites were performed. The effect of the addition of MAPP on the percolation network or distribution of SDCNC particles in HPP composites was evaluated. The changes in mechanical, crystallization and melting properties of resulting composites near the SDCNC percolation threshold were discussed after adding MAPP. Chapter 4 finally makes a conclusion based on the information obtained from the previous two Chapters and discusses potential future work to develop more ideal HPP composites with optimal performance.

Chapter 2 Material Properties of Spray-dried Cellulose Nanocrystal Reinforced Homopolymer Polypropylene Composites

2.1 Abstract

Spray-dried cellulose nanocrystal (SDCNC) particles have attracted intense interest as reinforcements in polymer composites because of their unique physical and mechanical properties. This work aims to develop homopolymer polypropylene (HPP) composites with different loading levels of SDCNC particles (5, 10, 15, and 30 wt.%) to understand their impact on composite mechanical, morphological, and thermal properties. The SDCNC-reinforced HPP composites were manufactured using a C.W. Brabender bowl internal mixer with a masterbatch concept and an injection molding process. The mechanical, morphological, and thermal properties of the composites were investigated. Compared to pure HPP, the tensile and flexural modulus of elasticity (MOE) of composites with 30 wt. % SDCNC significantly increased by up to 67% and 49%. The impact strength of the composites with the absence of a compatibilizer significantly increased by up to 19%, which was attributed to the mechanical interlocking network established between SDCNC particles and HPP. Additionally, increasing SDCNC loading in the composites led to higher crystallization peak temperatures and increased the degree of crystallinity (especially at 30 wt. % SDCNC content), indicating that the SDCNC particles can act as heterogeneous nucleating agents during the crystallization process. The thermal stability of the composite was slightly improved upon SDCNC introduction.

2.2 Introduction

Cellulose nanocrystals (CNCs), a type of nanomaterial extracted from lignocellulosic-based feedstocks, have a rod-like structure with diameters of 5 - 10 nm and lengths ranging from a few hundred nanometers to a few micrometers. [1] CNCs can be extracted from diverse lignocellulosic biomass sources by different mineral and organic acids hydrolysis methods and TEMPO-mediated oxidation, which determine the unique characteristics of CNCs. [2,3] After acid treatment, most of the amorphous regions of cellulose are removed, resulting in CNCs containing only a small amount of defects with a high degree of crystallinity, which makes CNCs possess remarkable mechanical properties. The modulus of elasticity and tensile strength of CNC are about 130 GPa and up to 10 GPa, respectively, which are significantly higher than those of natural fibers, such as kenaf, flax, cotton, and bamboo. [4,5] Additionally, CNCs have the benefits of high surface area, low density, non-toxicity, biodegradability, and renewability compared with synthetic fibers, such as glass fibers. [6] These characteristics of CNCs make it a promising candidate for reinforcing polymer composite materials.

Thermoplastic polymer composites reinforced by CNCs have attracted tremendous attention and improvements in the properties of many polar and nonpolar polymer matrices have been realized. [7-12] Polypropylene (PP) is the most widely used thermoplastic for commodity materials because of its favorable characteristics, including light weight, flexible processing techniques, and recyclability. [13-15] Compared to other commodity plastics, such as polyethylene, the higher melting point, chemical resistance, stiffness and rigidity, and heat resistance of PP make

it a popular choice as a matrix. [16] It was observed that adding CNCs to PP enhanced the mechanical and thermal properties when different process methods were used [9,17-19]. Bahar et al. [19] successfully prepared PP composites reinforced by CNCs at concentrations ranging from 5 to 15 wt.% via a solution casting process. They found that the tensile strength and Young's modulus of filled PP composites increased by about 81% and 19%, respectively. Sojoudiasli et al. [17] developed CNCs-reinforced PP composites by the melt compounding technique and observed that when compared with neat PP, tensile modulus of elasticty and strength of the composites with 2 wt.% CNCs was improved by about 30 % and 16 %, respectively. Both the solution casting and melt compounding methods are successful for developing composites with desirable performance. However, in order to meet the large-scale manufacturing that needs a cost- and energy-effective process, this study used the melt compounding approach because it is solvent-free and more flexible than solution casting when manufacturing nonpolar polymer matrix composites.

In practice, drying CNCs is a pre-requisite for melt compounding with polymers because CNCs are commonly obtained in the form of an aqueous suspension once other impurities and amorphous cellulose are removed from acid treatment solution. Various drying methods such as oven, freeze, spray, and supercritical drying have been evaluated. [20,21] The spray drying method has been suggested as the most appropriate technique for producing dried CNCs as fillers in composite manufacturing through a melt compounding process because of its simple process, rapidity, efficiency, low cost, and scalablity compared to other drying methods. [2,21-23] Notably, the morphologies of CNCs particles were changed from needle-like to donut-shaped or mushroom cap

structures after being subjected to spray drying. Changes in particle size from the nanoscale to the microscale was also demonstrated. [24] It is well-known that nanosized CNCs and freeze-dried CNCs exhibit great reinforcing ability in polymer composites. [25-27] The potential capability of spray-dried CNCs (SDCNCs) in improving the mechanical properties of polymer composites deserves to be explored.

CNCs can also be a promising toughening agent to improve polymer composite impact resistance that is one of the important mechanical characteristics determining the ability of a material to withstand fracture or failure under a load or impact. [8,12,13,28] This reinforcibility of CNCs particles can promote to addess the issue that the application of PP in structural applications where impact resistance is critical, such as in construction materials, automotive parts, or sporting equipment, is limited because of the low impact resistance of PP. A study reported that SDCNC particles increased the impact strength of PP composite from 21.96 to 24.2 J m^{-1} without any compatibilizer in the system. [29] However, the literature by Agarwal et al. [29] did not provide a clear explanation regarding the enhancement mechanism in impact resistance after incorporating SDCNC particles with the PP matrix, and did not study the effect of SDCNC particles at different loading levels on this performance. Herein, this work will pay close attention to the potential mechanism of the effect of SDCNC particles on the impact strength of PP composites. Simultaneously, the influence of CNCs in suspension format and dry format (freeze-, oven-, and spray freeze-dried CNCs) on crystallization behavior of polymer composites has been extensively studied, indicating that CNCs can act as a nucleating agent in polymer composites, forming a

transcrystalline layer around CNCs. [30-35] This research will investigate the effect of SDCNC particles on PP composites' crystallization behavior, which plays a significant role in determining the physical and mechanical behaviors of polymeric composites. In summary, it is essential to figure out the potential reinforcing ability of SDCNC particles in PP composite. Comprehending the fundenmental mechanism of the enhanced impact strength is vital for guiding to design and develop materials with tailored properties, expanding the opportunities of PP composites with improved properties.

The current work aims to understand the reinforcing effect of the irregularly shaped SDCNC particles with micrometer sizes on the behavior of PP composites. A melt compounding process was used to manufacture SDCNC-reinforced homopolymer polypropylene (HPP) composites with a masterbatch concept, which is an effective approach to achieve good dispersion of reinforcement in a polymer matrix. Meanwhile, the influence of SDCNC particles at different loading levels ranging from 5 to 30 wt.% on the composite properties was also examined. The research results indicated that SDCNC particles had a remarkable capability to improve the mechanical properties of PP composite with the absence of any compatibilizer. A possible mechanism explaining this enhancement was proposed. The thermal behaviors of SDCNC-reinforced PP composites were also discussed regarding crystallization characteristics and thermostability.

2.3 Materials and Methods

2.3.1 Materials

A commercial grade HPP with a density of 0.9 g cm^{-3} used as the matrix in this study was provided by ExxonMobil Chemical Company (ExxonMobil ™ PP1264E1, Houston, TX). The SDCNCs in the form of powder was supplied by CelluForce (Montreal, Canada). As reported by the supplier, the bulk density of SDCNC powder is 0.7 g cm^{-3}, and the crystalline fraction and specific surface area are 0.88 (by XRD) and 400 $m^2 g^{-1}$, respectively. In addition, the CNC powder has a sulfur content of 0.86 - 0.89 wt.%. The SDCNC powder was stored in a sealed container in the freezer before use.

2.3.2 SDCNC characterization

The particle size distribution of the SDCNCs was determined according to the process published in previous work. [36] The analysis was performed using a Mastersizer 2000 particle size analyzer (Malvern Instruments, Malvern, UK) with the Sirocco 2000 dry dispersion unit. The measurement was conducted at four-bar air pressure and 20 % feeder capacity. Three replicates were measured. The morphologies of SDCNC particles were examined using a Zeiss Evo 50VP scanning electron microscope (Oberkochen, Germany) operated at an accelerating voltage of 20 kV. The SDCNC particles were uniformly deposited on a conductive carbon tape, followed by sputter coating with gold for 60 s using a Q150R ES sputter coater (Hatfield, PA, USA) prior to the SEM characterization.

2.3.3 Preparation of CNC/HPP Composites

The HPP/SDCNC composites were prepared using a concept of masterbatch, which is an effective method to help the uniform dispersion of particles into polymer matrix. [36-38] The masterbatch with a high concentration of SDCNC particles (30 wt.% based on the weight of composites, the sum of the weights of SDCNC and HPP) was prepared in the first step. Then the masterbatch was diluted by adding fresh HPP pellets to reach the designed loading level of SDCNC. The resultant filled HPP composites are denoted as 5CNC, 10CNC, 15CNC, and 30CNC, representing the composites containing 5, 10, 15, and 30 wt.% SDCNC particles in HPP composite, respectively.

All masterbatch and final composites were prepared using a C.W. Brabender bowl mixer (CWB-2128, Hackensack, NJ, USA) with a maximum capacity of 200 grams operated at 200 °C with the two roller blades rotating counterclockwise at 60 RPM. For masterbatch composites manufacturing, the SDCNC particles were oven dried at 105 °C overnight to eliminate the potential moisture before melt compounding. HPP pellets were melted initially for 5 minutes in the mixer chamber. The SDCNC particles were then added slowly to the mixer. The mixture of SDCNC and HPP was then continued for another 5 minutes to obtain well-dispersed composites with stabilized mixing torque measured from the internal batch mixer. The composites were then removed from the mixer and solidified, followed by grinding into a pellet format using a low-speed granulator (Shini Plastic Technologies Inc., Willoughby, OH, USA) with a sieve size of 3 mm. For the final composite manufacturing, the masterbatch pellets were dry blended with fresh HPP pellets before

feeding to the internal mixer. The blended mixture was then mixed for 5 minutes. All composites containing SDCNC particles were dried overnight in an oven before each thermal processing at 105 °C. Pure HPP was manufactured using the same melt compounding procedure as the control sample.

The final composite pellets from each formulation were dried at 105 °C overnight and then injection molded (Proto-Ject 150HP, Manning Innovations Inc., Halls, TN, USA) into standard specimens with specific dimensions for tensile, impact, and flexure tests according to the ASTM standards D638 (Type IV), D256, D790, respectively. The injection molding machine was operated at barrel and nozzle temperatures of 200 °C. The impact and flexural samples were injection molded at 44 MPa and the tensile samples were injection molded at 53 MPa. The samples were kept in the mold for 10 seconds to pack during the injection molding process. The injection molded samples were then put into Ziploc bags and stored in desiccators at room temperature for at least 48 hours to avoid absorbing moisture before testing.

2.3.4 Composite mechanical property measurements

All mechanical property measurements were performed at 23 ± 2 °C with a relative humidity of 50 ± 5 %. Tensile tests were conducted according to ASTM D638 (Type IV) using a Mark-10 ESM750s motorized test machine (Copiague, NY, USA) with a 2,500-N load cell. An Epsilon extensometer SN E109112 (Jackson, WY, USA) was used to determine the strain of the test composites as the samples were stretched. The testing speed and nominal strain rate at the start of the test were 5 mm min^{-1} and 0.1 mm (mm $min)^{-1}$. Tensile strength (stress at yield point), tensile

strain (percentage elongation at yield), and tensile modulus of elasticity (MOE) were calculated from seven replicates and reported for neat HPP and all HPP/SDCNC composites. Flexural tests (three-point bending tests) were carried out according to ASTM D790-A using a Mark-10 ESM750s motorized test machine (Copiague, NY, USA) attached with a 500-N load cell. A support span length of 50 mm was employed. The speed of crosshead motion was 1.34 mm min^{-1} for all specimens. Five replicates were tested for each sample. Flexural strength and MOE for all samples were reported. The impact strength of all samples was evaluated according to ASTM D256 using an XJUD Digital Charpy Izod Impact Testing Machine (Deli Group CO. Ltd., Ningbo, China). All specimens were notched by a manual Instron CEAST notcher (Norwood, MA, USA) prior to impact tests according to the ASTM D256. Ten replicates were tested to calculate the average values of impact strengths in kg m^{-2} for all samples.

The mechanical properties, including tensile, flexural, and impact properties, were statistically analyzed with a 0.05 significance level using one-way ANOVA process. The fracture surfaces of impact-tested specimens were sputter-coated for examination using a Zeiss Evo 50VP scanning electron microscope (Oberkochen, Germany) operated at an accelerating voltage of 20 kV. Sputter coating was performed using a Q150R ES sputter coater (Hatfield, PA, USA) with gold for 60 s.

2.3.5 Water absorption tests

Water absorption tests were conducted using the impact fractured specimens to study the water resistance of the composites. The measurements were performed according to ASTM D570.

Initially, all specimens were dried at 105 °C in an oven to a constant weight. The initial sample weight and dimensions (thickness and width) were recorded to the nearest 0.0001 g using an electronic weighing balance (VWR-64B2, VWR, USA) and to the nearest of 0.001 mm using a digital micrometer (293-340-30, Mitutoyo, Japan). The thickness and width measurements were averaged from at least three points for each sample. The specimens were then immersed in containers filled with deionized water maintained at a room temperature of 23 ± 2 °C. The specimens were removed from the container daily for the first week, and then at one or two-week intervals, and extra water on the sample surface was wiped with tissue paper. The sample weight and dimensions were then immediately recorded. After each measurement, the specimens were immersed in the same containers. Five specimens were tested for each sample. The percentages of water gain, thickness swell, and width swell were calculated using the following equations:

$$\text{Water gain (\%)} = \frac{W_t - W_0}{W_0} \times 100 \quad (1)$$

$$\text{Thickness swell (\%)} = \frac{T_t - T_0}{T_0} \times 100 \quad (2)$$

$$\text{Width swell (\%)} = \frac{w_t - w_0}{w_0} \times 100 \quad (3)$$

Where W_0, T_0, and w_0 are the initial weight, thickness, and width of the specimens after oven-dried, W_t, T_t, and w_t are the weight, thickness, and width of specimens after immersion for different times, respectively.

2.3.6 Thermal properties

The crystallization and melting behaviors of all the composites were investigated using a DSC-250 differential scanning calorimeter (TA Instruments, DE, USA) under an N_2 atmosphere

with a flow rate of 50 ml min^{-1}. Samples of about 10-15 mg were sealed in a Tzero pan. The DSC measurement was carried out by heating the specimen from 40 °C to 200 °C, then maintaining it at 200 °C for 2 min to remove any previous thermal history. The specimen was then cooled to 40 °C at 10 °C min^{-1} to investigate their crystallization behaviors. Finally, the melting behaviors were characterized by reheating the specimen to 200 °C at 10 °C min^{-1}. Each sample was measured in triplicate. The TRIOS (TA Instruments, DE, USA) software was used to analyze all the data. The degree of crystallinity X_c (%) was calculated by the following equation:

$$X_c\ (\%) = \frac{\Delta H_m}{\Delta H_m^0\, w_{HPP}} \times 100\% \qquad (4)$$

Where ΔH_m is the measured melting enthalpy, ΔH_m^0 is the melting enthalpy of 100% HPP (205 J mol^{-1}), [39] and w_{HPP} is the weight fraction of HPP in the composite.

The thermostability of all the samples was characterized by thermogravimetric analysis (TGA) using a TGA-550 analyzer (TA Instruments, DE, USA). The measurement was carried out under nitrogen with flow rates of 60 ml min^{-1} and 40 ml min^{-1} for sample and balance purge, respectively. All samples (8-16 mg) were heated from 40 °C to 600 °C with a heating rate of 10 °C min^{-1}. Three replicates were tested for each sample. The TRIOS (TA Instruments, DE, USA) software was used to analyze the TGA and DTG (derivative thermogravimetric curve that is a plot of the rate of mass change with respect to temperature) curves.

2.3.7 Melt flow index (MFI)

The MFI measurements of pure HPP and HPP/SDCNC composites were performed using an MFI testing instrument (Techtongda, Markham, ON, Canada) in accordance with ASTM D1238.

The pellet samples of about 7 g obtained from the granulator were compacted and preheated for 4 min in the barrel. The MFI measurement was carried out at 200 °C with a constant load of 2.16 kg to keep SDCNC from thermal degradation during the measurement. Six replicates were collected and weighed for each sample.

2.4 Results and Discussion

2.4.1 The SDCNC particle characteristics

The volume-based particle size distribution of the SDCNC particles is shown in Figure 2-1A and a single peak with particle sizes ranging from 0.90 to 90 μm was obtained. The results indicated that the particle size at 10, 50, and 90 percentiles was 5.54 ± 0.14, 17.83 ± 0.13, and 38.72 ± 0.17 μm, i.e., 50% of the particles have a size smaller than 17.83 μm. The morphologies of SDCNC particles were characterized by SEM at different magnifications. The SDCNC particles possess irregular shapes with a broad range of sizes, as shown in Figure 2-1B. Some SDCNC particles are twisted or folded, forming large dense agglomerates with sizes of up to 40 μm. The SDCNC particles exhibit a mushroom cap or donut shape, similar to previous results. [24] The wrinkled profiles and cracks on the surface of SDCNC particles are also observed from the micrographs at high magnifications, as identified by the white arrows in Figure 2-1C-E. The irregular features of SDCNC particles are attributed to the influence of three fundamental forces, including hydrogen bonding, van der Waals forces, and capillary forces, experienced during the spray drying process. [20] These forces are responsible for governing individual CNC particles together, adhering to each other, and influencing the overall structure of dried particles.

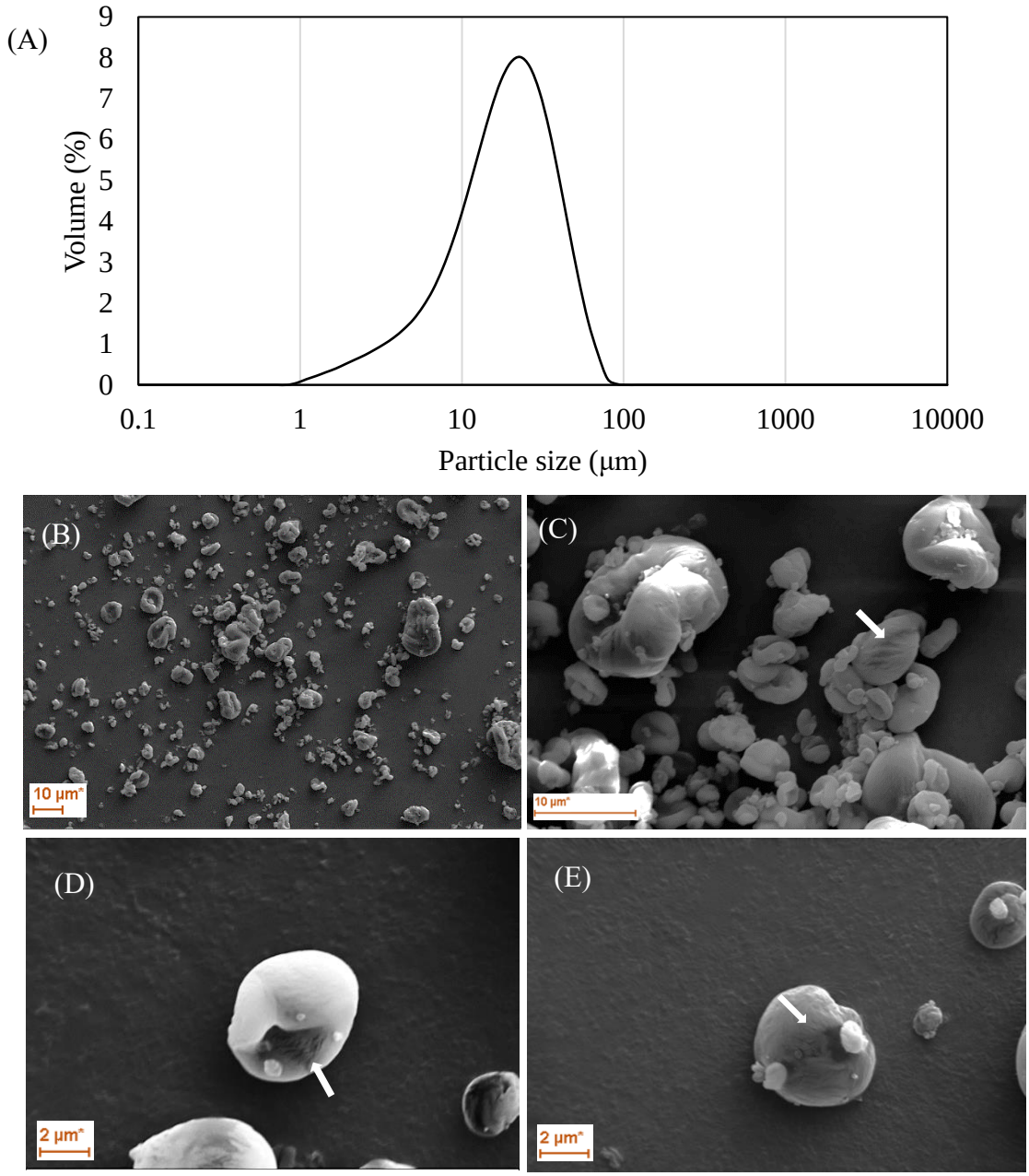

Figure 2-1 The particle size distribution of SDCNC particles (A) and the morphologies of SDCNC particles (B-E, , B: 1000X; C: 5000X; D and E: 8000X).

2.4.2 Mechanical Properties of the Composites

The mechanical performance of all composites was characterized, including tensile, flexural, and impact properties, according to the ASTM D638, D790, and D256, respectively. The statistical analysis results of all the composites' mechanical properties are summarized in Table 2-1.

The tensile properties were measured to determine the influence of different loadings of SDCNC particles on tensile MOE, strength, and strain. The properties of pure HPP and CNC/HPP composites are summarized in Table 2-1. The appearance of neat HPP was translucent, while the color of the composites became browner with the incremental loading levels of SDCNC in the composites. The color change may be ascribed to the presence of sulfate groups of the SDCNC particles in the composites, which are susceptible to thermal degradation at high temperatures in the thermal compounding and injection molding processes. [40] All the composites exhibit the same tendency under the tensile load, and the representative tensile stress-strain curves were recorded from the starting point to the yield point in the tensile test, as represented in Figure 2-2. Elastic deformation occurs initially within a small strain range with the highest deformation rate. The MOE is calculated based on the slope of this linear section of the stress-strain curve (zoom-in portion of the curve). Then, the stress-strain curve follows a viscoelastic deformation, where the deformation rate decreases, and the stress reaches a maximum value at the yield point.

The tensile strength of pure HPP is 30.2 ± 0.2 MPa, and the composite of 5CNC maintains the tensile strength at a similar level (30.4 ± 0.4 MPa). However, a significant reduction in tensile

strength of CNC/HPP composites at higher SDCNC loadings is observed (Table 2-1), although SDCNC particles possess a higher theoretical tensile strength (7.5-7.7 GPa) than HPP. [5] The tensile strength decreased to 29.1 ± 0.2, 26.9 ± 0.3 and 22 ± 0.7 MPa for the 10CNC, 15CNC, and 30CNC composites, which were 4, 11, and 27 % lower than that of neat HPP, respectively. This reduction is possibly attributable to the inherent incompatibility between hydrophilic SDCNC and hydrophobic HPP and the remarkably different surface energies of SDCNC (60.7 mJ m^{-2}) and HPP (around 30 mJ m^{-2}). [41,42] The incompatibility and varying surface energies result in the weak or no interfacial bonding between the two phases and the separated interface (as seen in the Figure 2-4, discussed in the following impact results section), which further lead to a lower stress transfer efficiency from the HPP matrix to the SDCNC particles under the applied tensile force.

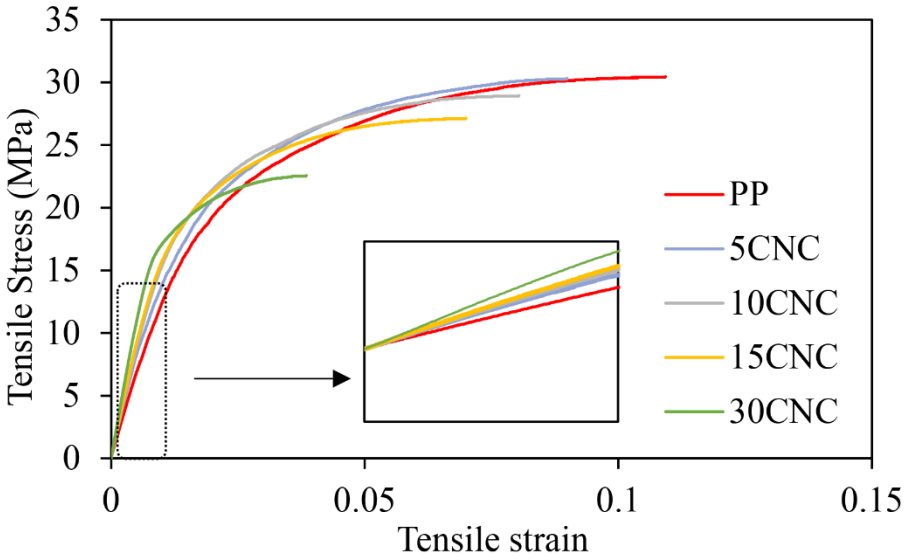

Figure 2-2 The representative tensile stress-strain curves of all the composites.

On the other hand, the tensile MOE of CNC/HPP composites progressively increases with increasing the SDCNC content (Table 2-1). The values of tensile MOE increased from 1.34 ± 0.03

GPa (HPP) to 1.66 ± 0.02, 1.76 ± 0.05, 1.86 ± 0.02, and 2.24 ± 0.16 GPa for the composites of 5CNC, 10CNC, 15CNC, and 30CNC, which are approximately 23, 31, 38, and 67% higher than that of pure HPP. The increase of MOE is caused by the higher stiffness of SDCNC (around 100-130 GPa) embedded in a lower MOE HPP matrix. [43] Incorporating SDCNC particles at high loadings in composites can decrease the plastic deformability of a polymer matrix while increasing the elastic response. [20]

Meanwhile, the tensile strain at yield gradually decreased from 10.3 ± 0.6% (HPP) to 8.5 ± 0.3, 7.5 ± 0.4, 7.1 ± 0.3, and 4.0 ± 0.2% for filled composites, which decreased by 18, 27, 31, and 62% relative to pure HPP (Table 2-1). This indicated a reduced ductility or more brittleness of HPP/SDCNC composites compared with neat HPP. The decrease of strain at yield for composites containing SDCNC can be explained not only by the poor interfacial adhesion between SDCNC and the HPP matrix in the absence of compatibilizer (Figure 2-4), but also by the decreased polymer molecular chain movement restricted by the SDCNC particles under the tensile load.

The flexural properties, including flexural strength and MOE, of the pure HPP and HPP/SDCNC composites are shown in Table 2-1. The representative flexural stress-strain curves are shown in Figure 2-3. Flexural strength is determined as the stress at the yield point for 30CNC and the stresses at 5% strain for pure HPP, 5CNC, 10CNC, and 15CNC composites since these composites did not yield or break within the 5% strain limit (Figure 2-3). The flexural MOE and strength of pure HPP are 1.32 ± 0.02 GPa and 40.7 ± 0.5 MPa, respectively. With the addition of

SDCNC particles into HPP, a similar trend to tensile MOE was observed for flexural MOE. Adding SDCNC particles in the HPP matrix significantly increased the flexural MOE because of the addition of SDCNC particles with a higher stiffness in HPP composites (Table 2-1). The values of flexural MOE for composites 10CNC, 15CNC, and 30CNC are 1.50 ± 0.02, 1.66 ± 0.07, and 1.96 ± 0.02 GPa, representing an increase of 14, 26, and 49% when compared to the neat HPP. The highest flexural strength is observed in the case of the 15CNC composite (44.2 ± 0.7 MPa), which is an enhancement of 8% as compared to pure HPP. There is no significant difference in flexural strength for 30CNC compared to HPP. The composites undergo a complex deformation during the flexural test, including the compression on the top surface and the tension on the bottom surface of composites. Higher stress is needed to reach 5% strain on the bottom surface for 10CNC and 15CNC than that required in pure HPP, thus increasing the flexural strength. [44]

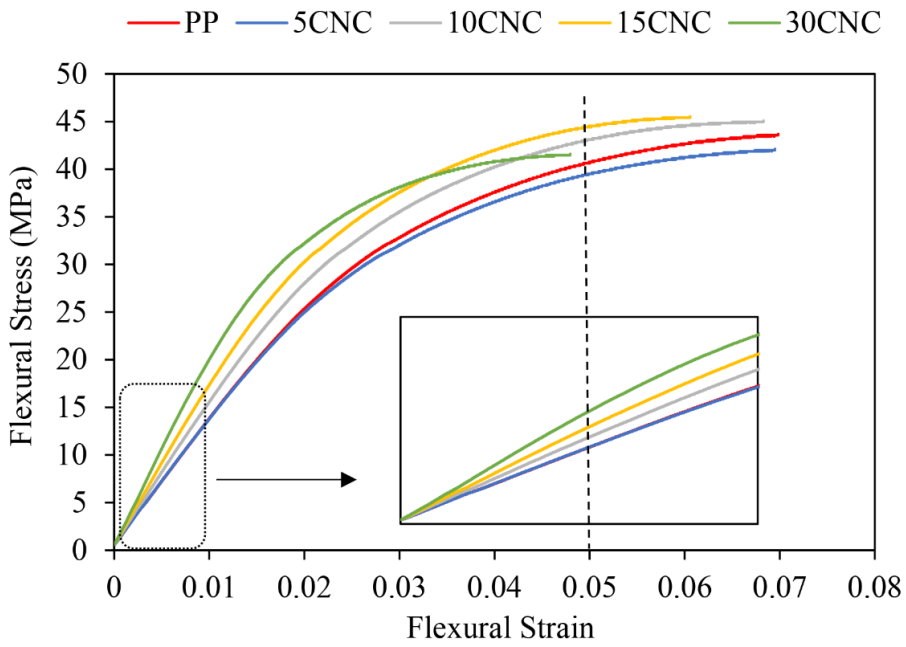

Figure 2-3 The representative flexural stress-strain curves of all the composites.

Table 2-1 The mechanical properties of SDCNC particles reinforced HPP composites.

Sample	Tensile Properties			Flexural Properties		Impact Strength ($kJ\ m^{-2}$)	Melt Flow Index ($g\ (10\ min)^{-1}$)
	MOE (GPa)	Strength (MPa)	Strain (%)	MOE (GPa)	Strength[c] (MPa)		
HPP	1.34±0.03[a] D[b]	30.2±0.2 A	10.3±0.6 A	1.32±0.02 D	40.7±0.5 C	1.62±0.12 B	7.04±0.07 A
5CNC	1.66±0.02 C	30.4±0.4 A	8.5±0.3 B	1.32±0.02 D	39.5±0.4 D	1.78±0.19 AB	6.77±0.07 B
10CNC	1.76±0.05 B	29.1±0.2 B	7.5±0.4 C	1.50±0.02 C	42.8±0.7 B	1.91±0.12 A	6.19±0.08 C
15CNC	1.86±0.02 B	26.9±0.3 C	7.1±0.3 C	1.66±0.07 B	44.2±0.7 A	1.92±0.13 A	6.22±0.10 C
30CNC	2.24±0.16 A	22.0±0.7 D	4.0±0.2 D	1.96±0.02 A	41.3±0.2[d] C	1.85±0.14 A	4.98±0.10 D

[a]Data were statistically analyzed by the average ± standard deviation.

[b]Values within a column with different letters, A, B, C, D, and E, indicate the significant difference at $P \leq 0.05$ between the samples. One way ANOVA followed with Tukey post-hoc process was used to statistically analyze all data.

[c]Flexural strength is reported by the stress at 5% strain since neither break nor yield occurred for pure HPP, 5CNC, 10CNC, 15CNC composite samples.

[d]Flexural strength of 30CNC composite is reported by the stress at the yield point.

The impact property determines the material deformation behavior when subjected to a high deformation rate. The results of notched Izod impact tests for all the composites are given in Table 2-1. The CNC/HPP composites demonstrate an improvement in impact resistance. The impact strength is 1.62 ± 0.12 kJ m^{-2} for pure HPP, and the values are 1.78 ± 0.19, 1.91 ± 0.12, 1.92 ± 0.13, and 1.85 ±0.14 kJ m^{-1} for 5CNC, 10CNC, 15CNC, and 30CNC composite, representing 10, 19, 19, and 15% enhancements as compared to pure HPP, respectively. The composite of 30CNC has a slightly lower value, but the number is still significantly higher than that of pure HPP. Adding SDCNC particles in HPP significantly improves the impact strength of CNC/HPP composites based on the statistical analysis compared to pure HPP. There is no significant change between composites with different content of SDCNC particles. This remarkable enhancement indicates that the SDCNC particles can absorb the impact energy when subjected to a high strain rate. [8] The morphologies of impact fractured surface of all CNC/HPP composites were investigated by SEM (Figure 2-4). Pure HPP behaves the typical homogenous polymer fractured surface, and the surface becomes rougher after adding rigid SDCNC particles, as shown in Figure 2-4. The coarser fracture surfaces indicate that more interfacial surface areas between SDCNC particles and HPP matrix were created by increasing the SDCNC loadings. Therefore, the composites can absorb more energy used for separating the interface. As a result, the impact strengths of all CNC/HPP composites are higher than that of pure HPP. Meanwhile, the relatively uniform distribution of SDCNC particles at low concentrate in the HPP matrix can be observed (Figure 2-4BDE). The SDCNC particle size after processing is closer to the initial size

(around 15 μm), no obvious larger agglomerates are formed. On the fracture surfaces of CNC/HPP composites, some SDCNC particles are embedded in the HPP matrix, while some SDCNC particles are pulled out from the matrix. The voids and the interfacial separation can be observed clearly (the white arrow in Figure 2-4D-F), mainly caused by the inherent incompatibility between hydrophilic SDCNC particles and hydrophobic HPP matrix.

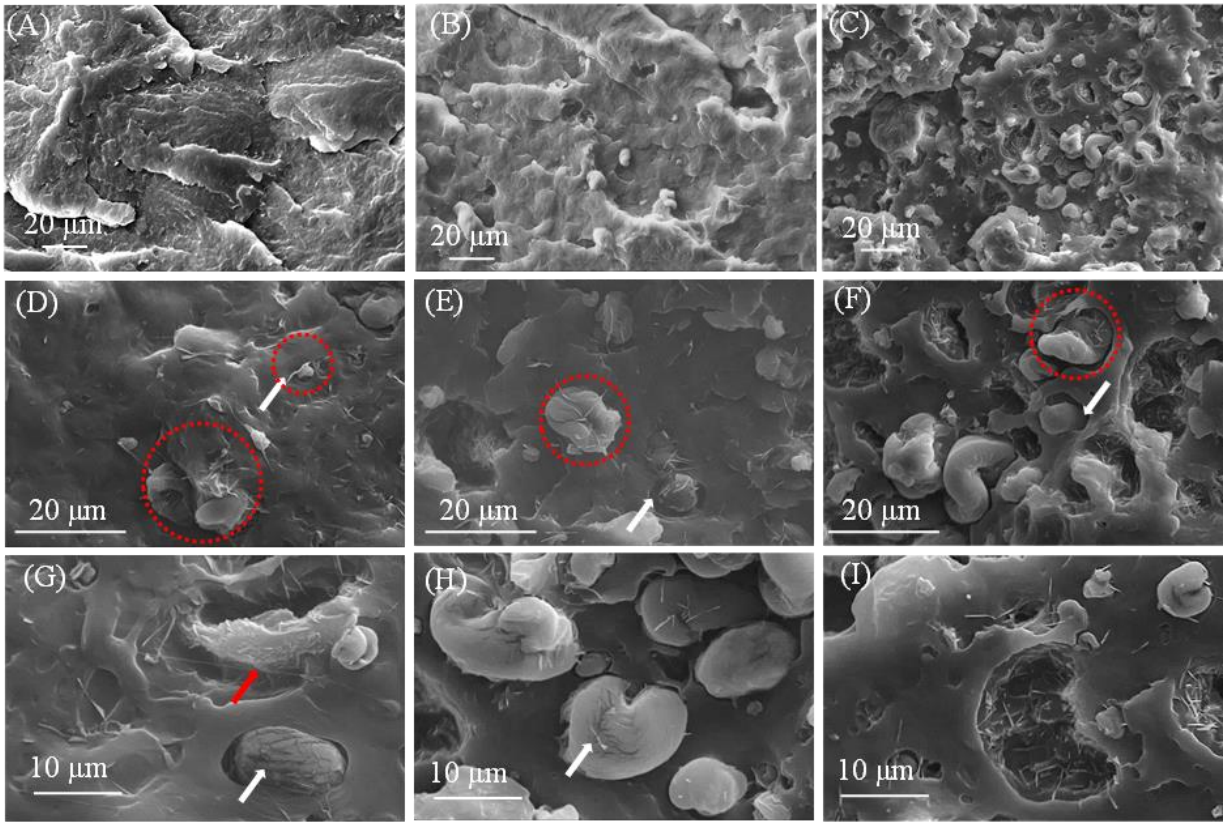

Figure 2-4 The SEM micrographs of fracture surfaces for pure HPP (A), 5CNC (B), 10CNC (D), 15CNC (E), 30CNC (CF) and the mechanical interlocking networks between SDCNC and polymer matrix (G-I). ABC: 2000X, DEF: 5000X, GHI: 8000X

Simultaneously, it is worth noting that from the red circles shown in Figure 2-4D-F, some stretched polymer filaments are strongly attached to the SDCNC surface after impact tests. This phenomenon can be explained by the theory of mechanical interlocking interfacial adhesion mechanism, where a strong interaction between two or more components was created by the physical interlocking. Polymer matrix can be filled in the holes or cracks on particle or fiber surface, subsequently, the two components can be locked mechanically after curing, enhancing the interfacial adhesion. [45] In this study, the melt HPP can penetrate and be locked into the cracks on the SDCNC during the composite solidification process, increasing the interfacial surface area and physical interaction between SDCNC and HPP and promoting the plastic deformation of the polymer matrix during impact testing. When composites are subjected to a high magnitude impact load with a high strain rate, the polymer phase in composites is stretched quickly and then breaks. The process will absorb more energy in fracturing the sample because of the mechanical interlocking network between the two phases. From the SEM micrographs with high magnification, more cracks can be distinctly observed on the SDCNC surface (The white arrow in Figure 2-4GH). A broken SDCNC agglomerate was also observed (The red arrow in Figure 2-4G), meaning greater energy is needed for the rupture of the CNC/HPP composites. Rough fracture surfaces (Figure 2-4I) are clearly identified after pulling out the embedded SDCNC particles from the matrix after the impact test, which indicates the formation of specific interfacial adhesion between SDCNC particles and HPP and supports the hypothesis that a mechanical interlocking network was established between SDCNC and HPP. In summary, the mechanical interlocking between the

SDCNC and HPP has a critical influence on the impact strength, compensating for the negative effect of the incompatibility between SDCNC and HPP. Therefore, a significant improvement in impact strength was achieved for CNC/HPP composites even without a compatibilizer in the system. However, for the 30CNC composite, the high SDCNC particle loadings generated much more discontinuous surfaces because of interfacial separation caused by the incompatibility (Figure 2-4C). More voids were also observed in the 30CNC composites (Figure 2-4C-F), which results in the lack of effective stress transfer from the HPP matrix to SDCNC particles and accelerates the de-bonding and the deformation. In this case, the impact strength of 30CNC composite is slightly lower than that of 15CNC, but it is still higher than pure HPP because of the mechanical interlocking network between SDCNC and HPP matrix.

2.4.3 Water absorption tests

The water absorption properties are important characteristics of composites that determine the potential end-use applications when exposed to environmental conditions. Water absorption in CNC-based composites was studied broadly. [7,46-49] The percentage of water gain against time for all composites is shown in Figure 2-5A. Similar behavior is observed for all the HPP/SDCNC composites. The water gain rate was rapid at the beginning of the immersion, then approached a plateau with a decreasing rate later. In some cases, especially for the 30CNC sample, it did not reach a plateau. The percentages of the water gain, thickness swell, and width swell for all composites after water immersion for 150 days are reported in Table 2-2. Each data point represents an average of five specimens.

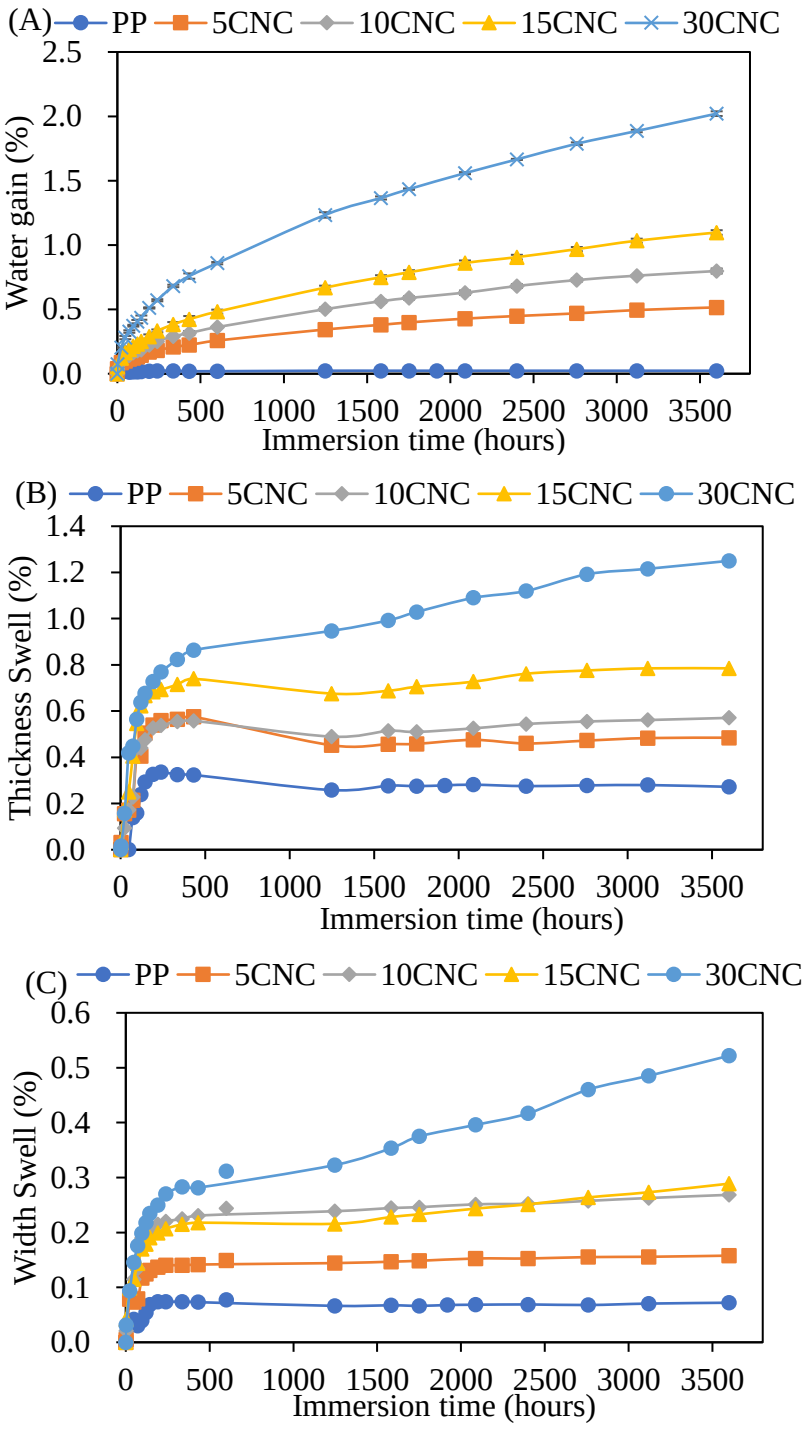

Figure 2-5 The long-term water gain (A), thickness swell (B), and width swell (C) for all composites.

Pure HPP absorbs the lowest level of water (0.02%) attributable to the hydrophobic nature of the material. The water gain of the HPP/SDCNC composites continuously increases with the increase in immersion time. Generally, moisture can penetrate into composites by three different mechanisms: 1) water molecules penetrate inside the micro-voids between polymer chains; 2) transportation of water molecules by micro-cracks in the matrix, formed in the compounding process; 3) diffusion into gaps and flaws at the interfaces between polymer and fillers. [50] The water gain of HPP/SDCNC composites is attributable not only to the hydroxyl groups in SDCNC that can attract water molecules through hydrogen bonding promoting water uptake, but also to the poor interfacial compatibility between SDCNC and HPP, generating the gaps in the interface (Figure 2-4D-F) and accelerating water collection. The amount of water gain depends upon the concentration of SDCNC particles in the composites - higher content of SDCNC particles results in higher water gain since SDCNC particles provide more binding sites for water. However, HPP/SDCNC composites showed little absorption after immersing water for 150 days (around 2 %), which was a strong indicator that the most of the SDCNC particles in composites are distributed uniformly encapsulated within the HPP matrix, preventing water molecules from penetrating and contacting the SDCNC particles.

A similar trend was observed for the thickness and width swell Figure 2-5BC. The dimensional swell in the thickness direction is higher than that in the width direction. The specimen width (around 12.7 mm) is much higher than the thickness (around 3.2 mm), water molecules have longer diffusion path from surface area to the center of composites along the width direction than

in the thickness direction, resulting in the slower rate of diffusion and lower dimension swell in width direction compared to that in thickness direction where diffusion occurred more rapidly. The overall dimensional swelling is low (less than 2%) for all HPP/SDCNC composites. This value is lower than that of other natural reinforcements in HPP polymer. For example, Ashori et al. [51] studied the effect of recycled newspaper fiber and wood flours as reinforcements on moisture absorption and thickness swelling behaviors for PP composites. The results showed that 30 wt.% reinforcements significantly influenced the water absorption (12%) and thickness swell (8.5%), which is approximately 6 times higher than that of HPP/SDCNC composites at the same concentration. In this respect, SDCNC particles as reinforcement in polymer composites behave better than other natural fibers when exposed to a wet environment for a long time.

Table 2-2 Water gain and dimensional swelling for pure HPP and CNC/HPP composites after immersion for 150 days (3600 hours).

Composite	Water gain (%)	Thickness Swell (%)	Width Swell (%)
HPP	0.02±0.01	0.27±0.05	0.07±0.05
5CNC	0.52±0.02	0.49±0.16	0.16±0.06
10CNC	0.80±0.02	0.57±0.19	0.27±0.04
15CNC	1.10±0.02	0.79±0.18	0.29±0.08
30CNC	2.02±0.02	1.25±0.25	0.52±0.12

2.4.4 Thermal properties of the composites

The DSC cooling and second heating thermograms of all the composites are shown in Figure 2-6. The melting and crystallization characteristic parameters, including melting enthalpy

(ΔH_m), onset temperature of melting ($T_{on\text{-}m}$), melting peak temperature (T_m), crystallization enthalpy (ΔH_c), onset temperature of crystallization ($T_{on\text{-}c}$), crystallization peak temperature (T_c), and degree of crystallinity (X_c %), are summarized in Table 2-3. The results clearly show that the addition of different levels of SDCNC to HPP only leads to a marginal influence on the T_m (± 1°C) as compared to pure HPP (Figure 2-6B), and it is not possible to establish a correlation between T_m and the SDCNC loading levels. Similar observations in the case of lignocellulosic material-reinforced HPP composites were reported. [17,52,53] However, it can be seen from Figure 2-6A that the $T_{on\text{-}c}$ and T_c of the composites gradually increase from 118.0 ± 0.3 °C to 127.2 ± 0.1°C and from 112.5 ± 0.1 °C to 123.0 ± 0.2 °C, respectively, as the SDCNC loading levels increased in HPP, which indicates that the crystallization of HPP started earlier during the cooling process. The temperature increase is probably because of the formation of a transcrystalline layer at the interface between SDCNC and HPP. [32,34,54] Another assumption is that the SDCNC particles within the HPP matrix can act as heterogeneous nucleating agents, allowing for many nucleation sites, promoting the partial crystalline growth of HPP and improving mechanical properties. [52] Meanwhile, as the loading of the SDCNC particles increases, the ΔH_c steadily decreases because a larger number of rigid particles in HPP restrict the thermal motion of polymer chains and reduce chain mobility for crystallization. [54] There is no significant change in X_c % of HPP after adding SDCNC particles except for the composite of 30CNC. The X_c % of HPP in 30CNC composite increases from 41.3 ± 0.9% (HPP) to 45.0 ± 1.0%. The increase in X_c % contributed to the decrease of the impact strength of 30CNC, which is demonstrated by the results in the mechanical property section.

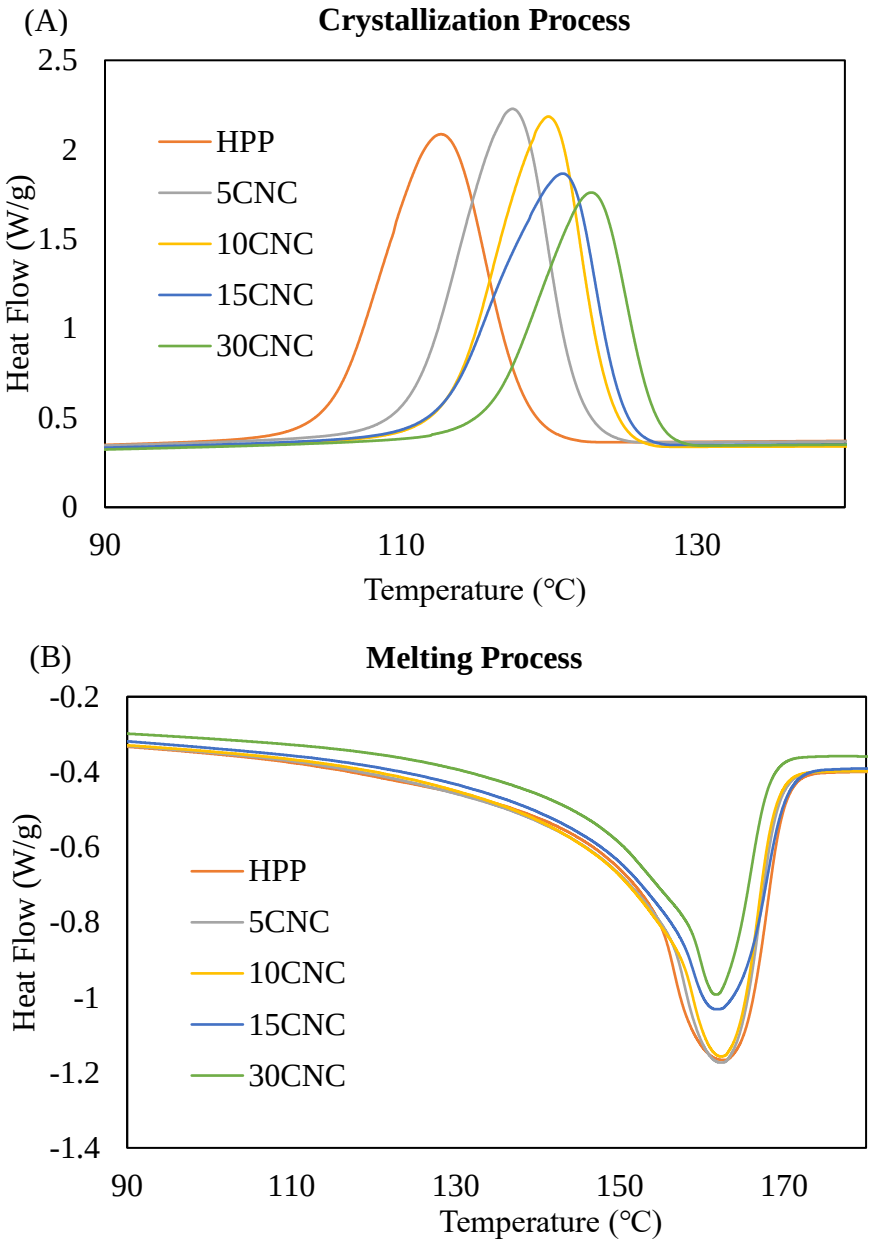

Figure 2-6 The DSC cooling (A) and second heating (B) curves of all the composites.

The thermostabilities of SDCNC and all the composites were investigated by TGA, and the TGA and DTG curves are shown in Figure 2-7. The TGA curve of the SDCNC can be divided into three sections. The initial weight loss of around 3 % occurred at temperatures ranging from 50 °C to 110 °C attributable to the evaporation of moisture from the material. [55] No actual thermal degradation took place in this step. The second major weight loss started at around 292 °C, which reached a dominant peak at around 305 °C on the DTG curve. This weight loss is attributed to cellulose degradation, including dehydration, depolymerization, decomposition of dehydrocellulose, and char residue formation. [56,57] The third weight loss occurred at around 350 °C because of the breakdown of char residues to low molecular weight products. [57] The residual weight at the end temperature of 600 °C for SDCNC is 18.1 ± 0.9 wt.%.

For pure HPP and HPP/SDCNC composites, the weight loss is less than 1 wt.% at 50 - 110 °C, indicating the trace amount of absorbed moisture in all composites. Based on the TGA and DTG curves, the HPP matrix displays a single-step thermal degradation behavior with an onset temperature of around 417 °C and a maximum weight loss rate at around 439 °C. The degradation of the HPP/SDCNC composites can be divided into two processes, as reported before, which are ascribed to the degradation of SDCNC (270 - 300 °C) and HPP (420 - 450 °C), respectively. [9,54,58] The other degradation process can be found from the DTG curves at around 150 °C for the 15CNC and 30CNC composites, which can be attributed to the presence of sulfate group in SDCNC introduced by the acid hydrolysis process in preparing the CNC material. [59,60] This degradation cannot be identified for 5CNC and 10CNC composites because of the low SDCNC content in the

composites. And it is also disappeared for the SDCNC particles from DTG curve. All composites used in the TGA measurements were subjected to the melt compounding process while the SDCNC particles are used in the native form, and the high temperature in the melt compounding process may facilitate the degradation of the SDCNC. This can be explained by the results that the onset temperature of SDCNC decreased from around 292 °C to around 280 - 285 °C and the peak temperature at the maximum weight loss rate decreased from around 305 °C to around 291 - 297 °C as shown in Table 2-4. The onset temperature for HPP/SDCNC composites are slightly greater than that of pure HPP indicating the improved thermal stability of HPP composites after introducing the SDCNC particles. This observation is consistent with the literature. [54] The residual weight at the end temperature of 600 °C for HPP is negligible, suggesting that HPP has a low thermal stability and char-forming ability. [61] It steadily increased for HPP/SDCNC composites with the increase of SDCNC content, indicating that the SDCNC particles can promote the formation of residual weight of HPP/SDCNC composites. [54]

2.4.5 Melt flow index

The MFI data for pure HPP and HPP/SDCNC composites are summarized in Table 2-1. The MFI of HPP is 7.04 ± 0.07 g/10 min. Adding SDCNC particles into HPP resulted in a lower MFI value, decreasing to 6.77 ± 0.07, 6.19 ± 0.08, 6.22 ± 0.10, and 4.98±0.10 g/10 min for 5CNC, 10CNC, 15CNC, and 30CNC, respectively. Incorporating rigid SDCNC particles into the polymeric matrix hinders the polymeric chain segments' rearrangement and free movement and

increases the composite viscosity. This result is similar to other literature in which the MFI value is reduced with increased natural reinforcement content in polymeric material. [62-65]

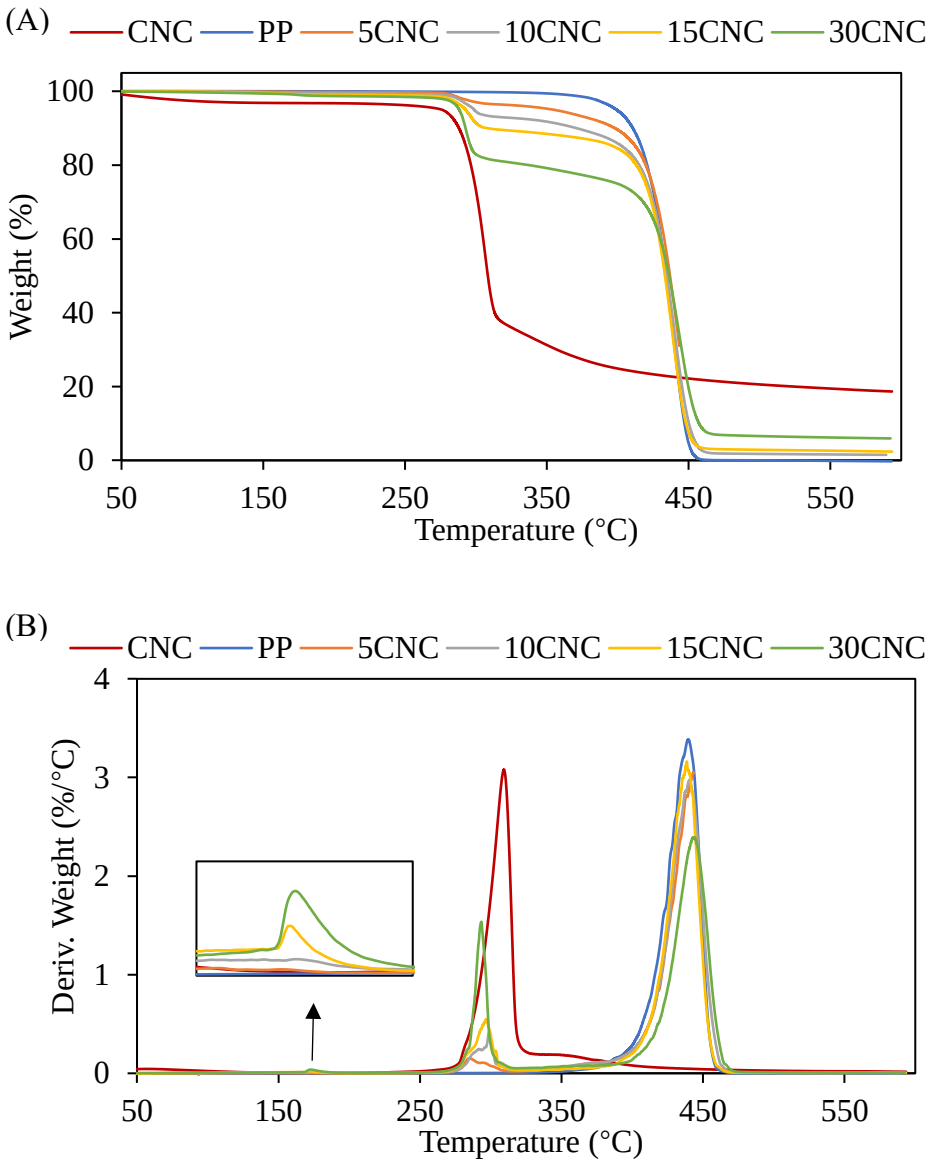

Figure 2-7 The TGA (A) and DTG (B) curves for all the samples.

Table 2-3. The melting and crystallization behaviors of all composites.

Samples	Melting process			Crystallization process			X_c (%)
	ΔH_m (J g^{-1})	$T_{on\text{-}m}$ (°C)	T_m (°C)	ΔH_c (J g^{-1})	$T_{on\text{-}c}$ (°C)	T_c (°C)	
HPP	84.7±1.8	151.0±0.3	161.6±0.9	87.0±1.1	118.0±0.3	112.5±0.1	41.3±0.9
5CNC	79.5±3.0	151.3±0.2	162.3±0.3	85.2±1.2	120.8±1.6	116.4±1.7	40.8±1.5
10CNC	76.3±1.1	151.3±0.5	162.5±0.3	80.6±2.4	124.3±0.2	120.3±0.4	41.4±0.6
15CNC	73.9±1.3	152.0±1.8	161.7±0.5	75.3±1.1	125.8±0.7	121.8±0.8	42.4±0.8
30CNC	64.5±1.5	153.6±1.5	161.5±0.1	64.6±0.1	127.2±0.1	123.0±0.2	45.0±1.0

Table 2-4. The TGA results for all the composites.

Samples	Region 1		Region 2		Region 3		Residual weight %	DTG Peak (°C)	
	Onset °C	Weight loss %	Onset °C	Weight loss %	Onset °C	Weight loss %		SDCNC	HPP
HPP	-	-	-	-	417.27	100.00	0.00	-	439.21
5CNC	-	-	279.46	4.46	421.07	94.90	0.66	291.28	438.77
10CNC	104.63	0.72	287.54	6.89	418.06	91.18	1.46	297.70	437.26
15CNC	116.66	0.85	285.74	8.82	420.73	88.23	2.25	294.48	439.12
30CNC	155.80	1.52	285.13	19.62	424.57	72.84	5.97	292.55	441.56

2.5 Conclusions

In the current work, the effect of the SDCNC particles and their loading levels on the mechanical, morphological, and thermal properties of HPP composites was investigated. The statistical analysis results showed that the mechanical properties of the HPP/SDCNC composites were highly impacted by the SDCNC particle loading level. Incorporating SDCNC particles in HPP composites significantly enhanced the tensile and flexural MOE. The impact strength of the HPP composites was significantly improved by adding SDCNC particles due to the presence of irregular-shaped SDCNC particles through the formation of the mechanical interlocking networks. The low water absorption and dimensional swell of HPP composites indicated that the composites can be properly used in applications where exposure to wet environment factor is a concern. The crystallization peak temperatures of the HPP/SDCNC composites increased with increasing SDCNC loading levels, suggesting the SDCNC particles can act as heterogeneous nucleating agents during the crystallization process. A slight improvement in the thermal stability of HPP composites after introducing SDCNC particles was observed. These findings have important implications for expanding the application of SDCNC in thermoplastic composites in specific fields, including packaging, construction, and automotive industries, and providing fundamental information to design and develop the composites with desired performance. However, tensile strength and strain at yield were adversely influenced because of the lack of any compatibilizer to improve the interfacial adhesion between the SDCNC particles and matrix. To address the

decreased tensile strength in this study and further improve the mechanical properties of the composites, the further work should enhance the compatibility between the SDCNC particles and HPP matrix by exploring the effect of coupling agents on the composite performance.

2.6 References

1. Hao W, Wang M, Zhou F, et al. A review on nanocellulose as a lightweight filler of polyolefin composites. *Carbohydrate polymers*. 2020;243:116466. doi:https://doi.org/10.1016/j.carbpol.2020.116466

2. Nagarajan K, Ramanujam N, Sanjay M, et al. A comprehensive review on cellulose nanocrystals and cellulose nanofibers: Pretreatment, preparation, and characterization. *Polymer Composites*. 2021;42(4):1588-1630. doi: https://doi.org/10.1002/pc.25929

3. Ganapathy V, Muthukumaran G, Sudhagar PE, et al. Mechanical properties of cellulose-based multiscale composites: A review. *Polymer Composites*. 2023;44(2):734-756. doi: https://doi.org/10.1002/pc.27175

4. Dufresne A. Nanocellulose: potential reinforcement in composites. *Natural polymers*. 2012;2:1-32.

5. Moon RJ, Martini A, Nairn J, Simonsen J, Youngblood JJCSR. Cellulose nanomaterials review: structure, properties and nanocomposites. *Chemical Society Reviews*. 2011;40(7):3941-3994. doi:https://doi.org/10.1039/C0CS00108B

6. Sabo RC, Elhajjar RF, Clemons CM, Pillai KM. Characterization and processing of nanocellulose thermosetting composites. *Handbook of Polymer Nanocomposites Processing, Performance and Application*. 2015;Volume C: Polymer Nanocomposites of Cellulose Nanoparticles:265-295.

7. Pandey J, Chu W, Kim C, Lee C, Ahn S. Bio-nano reinforcement of environmentally degradable polymer matrix by cellulose whiskers from grass. *Composites Part B: Engineering*. 2009;40(7):676-680. doi:https://doi.org/10.1016/j.compositesb.2009.04.013

8. Kargarzadeh H, Sheltami RM, Ahmad I, Abdullah I, Dufresne A. Cellulose nanocrystal: A promising toughening agent for unsaturated polyester nanocomposite. *Polymer*. 2015;56:346-357.

9. Khoshkava V, Kamal MR. Effect of cellulose nanocrystals (CNC) particle morphology on dispersion and rheological and mechanical properties of polypropylene/CNC nanocomposites. *ACS applied materials interfaces*. 2014;6(11):8146-8157. doi:https://doi.org/10.1021/am500577e

10. Kargarzadeh H, Mariano M, Huang J, et al. Recent developments on nanocellulose reinforced polymer nanocomposites: A review. *Polymer*. 2017;132:368-393. doi:https://doi.org/10.1016/j.polymer.2017.09.043

11. Alloin F, D'aprea A, Dufresne A, Kissi NE, Bossard F. Poly (oxyethylene) and ramie whiskers based nanocomposites: influence of processing: extrusion and casting/evaporation. *Cellulose*. 2011;18:957-973.

12. Sun M, Zhang L, Li C. Modified cellulose nanocrystals based on SI-ATRP for enhancing interfacial compatibility and mechanical performance of biodegradable PLA/PBAT blend. *Polymer Composites*. 2022;43(6):3753-3764. doi: https://doi.org/10.1002/pc.26653

13. Mousavi SR, Faraj Nejad S, Jafari M, Paydayesh A. Polypropylene/ethylene propylene diene monomer/cellulose nanocrystal ternary blend nanocomposites: Effects of different parameters on mechanical, rheological, and thermal properties. *Polymer Composites*. 2021;42(9):4187-4198. doi:https://doi.org/10.1002/pc.26137

14. Norrrahim MNF, Tengku Yasim-Anuar TA, Sapuan S, et al. Nanocellulose reinforced polypropylene and polyethylene composite for packaging application. *Bio-based Packaging: Material, Environmental Economic Aspects*. 2021:133-150. doi:https://doi.org/10.1002/9781119381228.ch8

15. Norrrahim MNF, Tengku Yasim-Anuar TA, Sapuan S, et al. Nanocellulose reinforced polypropylene and polyethylene composite for packaging application. *Bio-based Packaging: Material, Environmental and Economic Aspects*. 2021:133-150.

16. Dem K. Polyethylene vs Polypropylene: When to Choose What? The material selection platform. Accessed May 24, 2023. https://omnexus.specialchem.com/tech-library/article/polyethylene-versus-polypropylene

17. Sojoudiasli H, Heuzey MC, Carreau PJ. Mechanical and morphological properties of cellulose nanocrystal-polypropylene composites. *Polymer Composites*. 2018;39(10):3605-3617. doi:https://doi.org/10.1002/pc.24383

18. Ljungberg N, Bonini C, Bortolussi F, Boisson C, Heux L, Cavaillé J-Y. New nanocomposite materials reinforced with cellulose whiskers in atactic polypropylene: effect of

surface and dispersion characteristics. *Biomacromolecules*. 2005;6(5):2732-2739. doi:https://doi.org/10.1021/bm050222v

19. Bahar E, Ucar N, Onen A, et al. Thermal and mechanical properties of polypropylene nanocomposite materials reinforced with cellulose nano whiskers. *Journal of Applied Polymer Science*. 2012;125(4):2882-2889. doi:https://doi.org/10.1002/app.36445

20. Khoshkava V, Kamal M. Effect of drying conditions on cellulose nanocrystal (CNC) agglomerate porosity and dispersibility in polymer nanocomposites. *Powder Technology*. 2014;261:288-298. doi:https://doi.org/10.1016/j.powtec.2014.04.016

21. Peng Y, Gardner DJ, Han Y. Drying cellulose nanofibrils: in search of a suitable method. *Cellulose*. 2012;19:91-102.

22. Wang Q, Yao Q, Liu J, Sun J, Zhu Q, Chen H. Processing nanocellulose to bulk materials: A review. *Cellulose*. 2019;26:7585-7617.

23. Alarcón-Moyano J, Acuña D, Matiacevich S, et al. Physico-chemical and structural characterization of cellulose nanocrystals obtained by two drying methods: Freeze-drying and spray-drying. *Food Hydrocolloids*. 2023;140:108571. doi:https://doi.org/10.1016/j.foodhyd.2023.108571

24. Peng Y, Han Y, Gardner DJ. Spray-drying cellulose nanofibrils: Effect of drying process parameters on particle morphology and size distribution. *Wood and Fiber Science*. 2012:448-461.

25. Tanpichai S, Oksman K. Cross-linked nanocomposite hydrogels based on cellulose nanocrystals and PVA: Mechanical properties and creep recovery. *Composites Part A: Applied Science and Manufacturing*. 2016;88:226-233.

26. Xu X, Liu F, Jiang L, Zhu J, Haagenson D, Wiesenborn D. Cellulose nanocrystals vs. cellulose nanofibrils: a comparative study on their microstructures and effects as polymer reinforcing agents. *ACS applied materials and interfaces*. 2013;5(8):2999-3009.

27. DiLoreto E, Haque E, Berman A, Moon RJ, Kalaitzidou K. Freeze dried cellulose nanocrystal reinforced unsaturated polyester composites: challenges and potential. *Cellulose*. 2019;26:4391-4403.

28. Zhang X, Zhang Y. Reinforcement effect of poly (butylene succinate)(PBS)-grafted cellulose nanocrystal on toughened PBS/polylactic acid blends. *Carbohydrate polymers*. 2016;140:374-382. doi:https://doi.org/10.1016/j.carbpol.2015.12.073

29. Agarwal J, Mohanty S, Nayak SK. Valorization of pineapple peel waste and sisal fiber: Study of cellulose nanocrystals on polypropylene nanocomposites. *Journal of Applied Polymer Science*. 2020;137(42):49291. doi:https://doi.org/10.1002/app.49291

30. Kang H, Kim DS. A study on the crystallization and melting of PLA nanocomposites with cellulose nanocrystals by DSC. *Polymer Composites*. 2023:1-10. doi:https://doi.org/10.1002/pc.27658

31. Siqueira G, Bras J, Dufresne A. Cellulose whiskers versus microfibrils: influence of the nature of the nanoparticle and its surface functionalization on the thermal and mechanical

properties of nanocomposites. *Biomacromolecules*. 2009;10(2):425-432. doi:https://doi.org/10.1021/bm801193d

32. Khoshkava V, Ghasemi H, Kamal MR. Effect of cellulose nanocrystals (CNC) on isothermal crystallization kinetics of polypropylene. *Thermochimica Acta*. 2015;608:30-39. doi:https://doi.org/10.1016/j.tca.2015.04.007

33. Corrêa AC, Teodoro KBR, Simão JA, et al. Cellulose nanocrystals from curaua fibers and poly [ethylene-co-(vinyl acetate)] nanocomposites: Effect of drying process of CNCs on thermal and mechanical properties. *Polymer Composites*. 2020;41(5):1736-1748. doi: https://doi.org/10.1002/pc.25493

34. Gray DG. Transcrystallization of polypropylene at cellulose nanocrystal surfaces. *Cellulose*. 2008;15:297-301.

35. Kamal MR, Khoshkava V. Effect of cellulose nanocrystals (CNC) on rheological and mechanical properties and crystallization behavior of PLA/CNC nanocomposites. *Carbohydrate polymers*. 2015;123:105-114. doi:https://doi.org/10.1016/j.carbpol.2015.01.012

36. Peng Y, Gallegos SA, Gardner DJ, Han Y, Cai Z. Maleic anhydride polypropylene modified cellulose nanofibril polypropylene nanocomposites with enhanced impact strength. *Polymer composites*. 2016;37(3):782-793. doi:https://doi.org/10.1002/pc.23235

37. Wang L, Roach AW, Gardner DJ, Han Y. Mechanisms contributing to mechanical property changes in composites of polypropylene reinforced with spray-dried cellulose nanofibrils. *Cellulose*. 2018;25:439-448.

38. Bagheriasl D, Carreau P, Dubois C, Riedl B. Properties of polypropylene and polypropylene/poly (ethylene-co-vinyl alcohol) blend/CNC nanocomposites. *Composites Science Technology*. 2015;117:357-363. doi:https://doi.org/10.1016/j.compscitech.2015.07.012

39. Aumnate C, Rudolph N, Sarmadi M. Recycling of polypropylene/polyethylene blends: Effect of chain structure on the crystallization behaviors. *Polymers*. 2019;11(9):1456. doi:https://doi.org/10.3390/polym11091456

40. Voronova M, Surov O, Zakharov A. Nanocrystalline cellulose with various contents of sulfate groups. *Carbohydrate polymers*. 2013;98(1):465-469. doi:https://doi.org/10.1016/j.carbpol.2013.06.004

41. Brewis D, Briggs D. Adhesion to polyethylene and polypropylene. *Polymer*. 1981;22(1):7-16. doi:https://doi.org/10.1016/0032-3861(81)90068-9

42. Shang W, Huang J, Luo H, Chang PR, Feng J, Xie G. Hydrophobic modification of cellulose nanocrystal via covalently grafting of castor oil. *Cellulose*. 2013;20(1):179-190.

43. Dufresne A. Nanocellulose: a new ageless bionanomaterial. *Materials today*. 2013;16(6):220-227.

44. Peng Y, Musah M, Via B, Wang X. Calcium carbonate particles filled homopolymer polypropylene at different loading levels: mechanical properties characterization and materials failure analysis. *Journal of Composites Science*. 2021;5(11):302.

45. Zheng H, Zhang W, Li B, et al. Recent advances of interphases in carbon fiber-reinforced polymer composites: A review. *Composites Part B: Engineering*. 2022;233:109639. doi:https://doi.org/10.1016/j.compositesb.2022.109639

46. Garcia de Rodriguez NL, Thielemans W, Dufresne A. Sisal cellulose whiskers reinforced polyvinyl acetate nanocomposites. *Cellulose*. 2006;13(3):261-270.

47. Mathew AP, Gong G, Bjorngrim N, Wixe D, Oksman KS. Moisture absorption behavior and its impact on the mechanical properties of cellulose whiskers-based polyvinylacetate nanocomposites. *Polymer Engineering and Science*. 2011;51(11):2136-2142. doi:https://doi.org/10.1002/pen.22063

48. Li VC-F, Kuang X, Mulyadi A, Hamel CM, Deng Y, Qi HJ. 3D printed cellulose nanocrystal composites through digital light processing. *Cellulose*. 2019;26(6):3973-3985.

49. Samarasekara A, Kumara S, Madhusanka A, Amarasinghe D, Karunanayake L. Study of thermal and mechanical properties of microcrystalline cellulose and nanocrystalline cellulose based thermoplastic material. IEEE; 2018:465-470.

50. Espert A, Vilaplana F, Karlsson S. Comparison of water absorption in natural cellulosic fibres from wood and one-year crops in polypropylene composites and its influence on their mechanical properties. *Composites Part A: Applied science manufacturing*. 2004;35(11):1267-1276. doi:https://doi.org/10.1016/j.compositesa.2004.04.004

51. Ashori A, Sheshmani S. Hybrid composites made from recycled materials: moisture absorption and thickness swelling behavior. *Bioresource technology*. 2010;101(12):4717-4720. doi:https://doi.org/10.1016/j.biortech.2010.01.060

52. Amash A, Zugenmaier P. Morphology and properties of isotropic and oriented samples of cellulose fibre–polypropylene composites. *Polymer*. 2000;41(4):1589-1596. doi:https://doi.org/10.1016/S0032-3861(99)00273-6

53. Agarwal J, Mohanty S, Nayak SK. Influence of cellulose nanocrystal/sisal fiber on the mechanical, thermal, and morphological performance of polypropylene hybrid composites. *Polymer Bulletin*. 2021;78:1609-1635.

54. Shin H, Kim S, Kim J, Kong S, Lee Y, Lee JC. Preparation of 3-pentadecylphenol-modified cellulose nanocrystal and its application as a filler to polypropylene nanocomposites having improved antibacterial and mechanical properties. *Journal of Applied Polymer Science*. 2022;139(13):51848. doi:https://doi.org/10.1002/app.5184

55. Lamaming J, Hashim R, Sulaiman O, Leh CP, Sugimoto T, Nordin NA. Cellulose nanocrystals isolated from oil palm trunk. *Carbohydrate Polymers*. 2015;127:202-208. doi:https://doi.org/10.1016/j.carbpol.2015.03.043

56. Roman M, Winter WT. Effect of sulfate groups from sulfuric acid hydrolysis on the thermal degradation behavior of bacterial cellulose. *Biomacromolecules*. 2004;5(5):1671-1677. doi:https://doi.org/10.1021/bm034519+

57. Peng Y, Gardner DJ, Han Y, Kiziltas A, Cai Z, Tshabalala MA. Influence of drying method on the material properties of nanocellulose I: thermostability and crystallinity. *Cellulose*. 2013;20(5):2379-2392.

58. Qiu W, Zhang F, Endo T, Hirotsu T. Preparation and characteristics of composites of high-crystalline cellulose with polypropylene: Effects of maleated polypropylene and cellulose content. *Journal of Applied Polymer Science*. 2003;87(2):337-345. doi:https://doi.org/10.1002/app.11446

59. Kim D-Y, Nishiyama Y, Wada M, Kuga S. High-yield carbonization of cellulose by sulfuric acid impregnation. *Cellulose*. 2001;8(1):29-33.

60. Prado KS, Spinacé MA. Isolation and characterization of cellulose nanocrystals from pineapple crown waste and their potential uses. *International journal of biological macromolecules*. 2019;122:410-416.

61. Yu Y, Fu S, Song Pa, et al. Functionalized lignin by grafting phosphorus-nitrogen improves the thermal stability and flame retardancy of polypropylene. *Polymer degradation stability*. 2012;97(4):541-546. doi:https://doi.org/10.1016/j.polymdegradstab.2012.01.020

62. Haq S, Srivastava R. Wood polypropylene (PP) composites manufactured by mango wood waste with virgin or recycled PP: mechanical, morphology, melt flow index and crystalline behaviour. *Journal of Polymers and the Environment*. 2017;25(3):640-648.

63. Jam NJ, Behravesh AH. Flow behavior of HDPE-fine wood particles composites. *Journal of Thermoplastic Composite Materials*. 2007;20(5):439-451.

64. Kumari R, Ito H, Takatani M, Uchiyama M, Okamoto T. Fundamental studies on wood/cellulose-plastic composites: effects of composition and cellulose dimension on the properties of cellulose/PP composite. *Journal of wood science*. 2007;53(6):470-480.

65. Fonseca-Valero C, Ochoa-Mendoza A, Arranz-Andrés J, González-Sánchez C. Mechanical recycling and composition effects on the properties and structure of hardwood cellulose-reinforced high density polyethylene eco-composites. *Composites Part A: Applied Science and Manufacturing*. 2015;69:94-104.

Chapter 3 Percolation Threshold of Spray-dried Cellulose Nanocrystal in Homopolymer Polypropylene Composite: the Effect on Mechanical and Thermal Properties

3.1 Abstract

Understanding the percolation threshold is essential for determining composites' performance and ensuring efficient material usage in different applications. Spray-dried cellulose nanocrystals (SDCNC) reinforced homopolymer polypropylene (HPP) composites at 20, 30, 40, and 50 wt. % were prepared to investigate the percolation threshold of SDCNC particles in HPP and assess the effect of the percolation threshold on the mechanical and thermal properties of resultant composites. The effect of a compatibilizer, maleic anhydride polypropylene (MAPP) at 3, 5, and 7wt. %, on the SDCNC particles percolation networks and composites performance were also studied. The results indicated that SDCNC particle percolation networks in HPP were established at 30 – 40 wt.% SDCNC loading. Water absorption results confirmed this observation and indicated that adding MAPP influenced the percolation network. Without MAPP, the impact strength significantly increased before the percolation threshold and declined beyond it. HPP's crystallization behavior changed due to the SDCNC partiles' nucleation function until a saturated nucleation function at the percolation threshold. Introducing MAPP significantly improved tensile strength (58%), tensile strain (61%), flexural strength (45%), and impact strength (91%) compared with the corresponding composites without MAPP, attributed to the enhanced interfacial adhesion between the SDCNC particles and HPP.

3.2 Introduction

The broad range of applications of polypropylene (PP), including packaging, automobile, construction, toys, and furniture, makes it one of the most utilized commodity thermoplastic polymers due to its excellent barrier properties, moisture and chemical resistance, lightweight, sterilizability, moldability, and durability. [1-3] However, it has some limitations that should be considered in various applications, such as low impact strength, making it prone to brittle failure. To overcome the uncompetitive mechanical property and increase the usage of PP, synthetic or natural reinforcements or fillers are used to enhance its mechanical performance, including toughness. Synthetic fillers such as glass or carbon fibers, talc, calcium carbonate, nanoclay, and carbon nanotubes have been widely studied for reinforcing PP composites. [4-9] Recently, there has been a growing focus on environmental concerns, leading to increased interest in incorporating natural fillers in PP composites, such as wood flour, jute, rice husks, and cellulose fibers. Spray-dried cellulose nanocrystal (SDCNC) particles, a dry form of cellulose nanocrystal (CNC), have shown promise in fabricating PP composites at an industrial scale via a cost-effective and solvent-free melt compounding process. [10] The one challenge in developing satisfactory PP composites with SDCNC particles is the inherent incompatibility between the hydrophilic nature of SDCNC and the hydrophobic nature of PP, leading to poor interfacial adhesion between the components, a key factor influencing the tensile strength of composites. [11] Maleic anhydride polypropylene (MAPP) is commonly used to effectively increase the interfacial adhesion between cellulosic

fillers and PP matrix in the composite industry due to the low cost, simple process, and absence of extra solvents compared to other chemical surface treatments. [2,12-14]

The high reinforcing performance of composites is ascribed not only to the strong interfacial adhesion between CNC and the matrix but also to the formation of a percolation network of CNC in composites. [15,16] Percolation describes the dispersion of particles (like CNCs) in a random system to form larger connected clusters spanning across the entire system at a certain critical volume fraction, which is referred to as the percolation threshold. [17] The CNC percolation threshold is crucial for its reinforcing effect on composites. Below the threshold, separated particles cannot form a network, and the optimal reinforcing capacity of CNC thus cannot be achieved. At the percolation threshold value, CNCs are in contact with each other, creating a rigid continuous percolation network via the interaction between the abundant hydroxyl groups on the CNC surface, forming a hydrogen-bonded solid structure with high strength to reinforce the composites. Surpassing the percolation threshold leads to CNC agglomeration, inducing stress concentration points and weakening the effective stress transfer from CNC to the matrix. [18]

Existing literature showed that nanosized rod-like CNC can dramatically improve the performance of polymer composites by building a continuous rigid network through the formation of hydrogen bonds. [19-23] Corder and coworkers studied CNC percolation in the aqueous photoactive poly (vinyl alcohol) derivative (PVA-SbQ) solution by investigating the rheological properties of the nanocomposites. [19] They found that above 1.5 wt. % CNC concentration in composites, several changes in rheological behavior were observed. Storage modulus (G′) sharply

increased during the *in situ* photocrosslinking experiments. Santamaria-Echart et al. evaluated the CNC percolation threshold in a waterborne polyurethane matrix by the measurement of tensile properties and thermomechanical properties of resulting nanocomposites. [22] In this study, remarkable enhancements in tensile stress at yield (36%), modulus (16%), and thermomechanical stability were achieved at the CNC percolation threshold (3 wt. % CNC). The mechanical and thermomechanical properties decreased above the CNC percolation threshold (5 wt. % CNC) because of the formation of CNC agglomerates. Sheets of styrene butadiene rubber (SBR) reinforced with varying contents of CNC from 0.5 to 8 wt.% (based on rubber weight) were fabricated by a solution casting process. [20] The tear strength and maximum work required to tear the sheets increased above 4 wt.% of CNC in SBR latex, where the percolation of CNC occurred.

From the literature discussed above, the prediction of percolation threshold in a specific polymer matrix mainly focuses on the rod-like CNC and is primarily performed in the solution casting/evaporation process, where particles can be uniformly dispersed in a polymer matrix, which is an essential requirement for creating an ideally percolated network in composites. [17] Simultaneously, hydrogen bonding networks can be established during the solution casting process with solvent drying. [24] However, for SDCNC dispersed in a thermoplastic compounded with a melt process, the hydrogen bonding network of SDCNC is hard to build because no solvent is involved. Research on the SDCNC percolation threshold in a nonpolar PP matrix when using a melt compounding process to manufacture composites is of interest to academia and industry. The majority of studies have determined the experimental percolation threshold of CNC based on

mechanical or rheological properties, as mentioned above. In this study, we developed a novel method to identify the experimental percolation threshold of SDCNC in PP composites by investigating the water absorption behaviors of composites.

The main objective of this research was to search the SDCNC percolation threshold within HPP composites by studying the characterization of water absorption of SDCNC-reinforced HPP composites. Three hypotheses were involved in this research: (1) the percolation threshold of SDCNC particles in HPP composites can be identified by characterizing the moisture absorption behaviors of the SDCNC particle reinforced HPP composites; (2) the mechanical properties of the SDCNC particle reinforced PP composites decrease significantly at the percolation threshold due to the incapability of establishing hydrogen bonds between SDCNC particles; and (3) compatibilization between SDCNC particles and polymer matrix can significantly change the mechanical properties of the composites, even at SDCNC loading levels above the percolation threshold. The fundamental knowledge the hypothesis statement provides helps design high-performance composite systems using renewable resources. The mechanical behaviors of the composites, including tensile, flexural, and impact properties, were examined. A compatibilizer of MAPP was used to establish the bonding between SDCNC particles and the HPP matrix and improve their interfacial adhesion. The effect of MAPP on the mechanical and thermal behaviors of HPP composites near the SDCNC percolation threshold was assessed as well. The results indicated that the SDCNC percolation network started to form at the loading level between 30 - 40 wt.%. Flexural and impact strength were significantly improved before reaching the percolation

threshold, even without the compatibilizer in the composites, followed by decreasing above the threshold. The crystallization peak temperature increased with the increasing loading level of SDCNC and remained constant above the SDCNC percolation threshold value. Introducing MAPP into the system significantly changed the mechanical properties of the composite by establishing adhesion between SDCNC and the polymer matrix. Simultaneously, MAPP covered the SDCNC particle surface, reducing the nucleation function of SDCNC on the HPP matrix. The HPP crystallization peak temperature increase caused by SDCNC was also depressed by the incorporation of MAPP.

3.3 Materials and methods

3.3.1 Materials

HPP pellets (ExxonMobil ^{TM} PP1264E1) with a density of 0.9 g cm^{-3} were received from ExxonMobil Chemical Company (Houston, TX). The SDCNC powder derived by sulfuric acid hydrolysis was obtained from CelluForce (Montreal, Canada). MAPP (Polybond 3200) pellets were supplied by ChemPoint Inc. (Bellevue, WA, USA). It has a melt flow index of 115 g 10 min^{-1} (190 °C/2.16 Kg), a density of 0.91 g cm^{-3}, and a melting point of 157 °C. The maleic anhydride content is in the range of 0.8 - 1.2 %.

3.3.2 Composites manufacturing

A masterbatch method was used to prepare SDCNC-reinforced HPP composites with or without MAPP pellets. A C.W. Brabender internal mixer (CWB-2128, Hackensack, NJ, USA) at

200 °C with the two mixing blades rotating counterclockwise at 60 rpm was used to manufacture all composites. The SDCNC powder and MAPP pellets were oven-dried at 105 °C overnight to remove any potential moisture before melt compounding. The HPP pellets were first melted in the mixer until a constant torque was achieved (5 minutes). Then the SDCNC particles were added into the mixing chamber for further compounding for an additional 5 min to reach a constant torque value of the mixer. The masterbatch with 50 wt.% SDCNC was prepared first. The masterbatch for the composite with MAPP was prepared by mixing HPP and the designated amount of MAPP first, followed by adding the SDCNC particles. After thermal compounding, the cooled mixture was ground into a pellet form using a granulator (Shini Plastic Technologies Inc., Willoughby, OH, USA). For the fabrication of the final composites according to the formulations shown in Table 3-1, the oven-dried masterbatch pellets and the designed amount of fresh HPP pellets were dry-mixed and then fed into the mixer for thermal compounding for 5 minutes until a well-dispersed final composite was obtained, as indicated by a constant torque value. The final mixed composites were then ground into pellets and oven-dried at 105 °C overnight prior to being processed into standard-shaped samples for mechanical properties evaluation according to ASTM D638 (Type IV), ASTM D790-A, and ASTM D256, respectively. An injection molding machine (Proto-Ject 150HP, Manning Innovations Inc., Halls, TN, USA) at 200 °C and a pressure of 44 MPa was used for all composite specimen manufacturing. After molding, the samples were placed in Ziploc bags and stored in desiccators at room temperature for at least 48 hours to prevent moisture absorption before the test. Pure HPP pellets prepared with the same melt compounding and injection molding

process were used as a control sample. The sample names are listed in Table 3-1, where SDCNC-reinforced HPP composites without MAPP (CNC/HPP) pellets were denoted as aCNC (a is the SDCNC weight percentage in the composite based on the total weight of composite), and SDCNC-reinforced HPP composites with MAPP pellets (CNC/MAPP/HPP) was denoted as bCNCcMAPP (b and c are the SDCNC and MAPP weight percentages based on the total weight of the composite).

Table 3-1. The formulations of CNC/HPP and CNC/MAPP/HPP composites.

Sample denotation	HPP (wt.%)	SDCNC (wt.%)	MAPP (wt.%)
HPP	100	0	0
20CNC	80	20	0
30CNC	70	30	0
40CNC	60	40	0
50CNC	50	50	0
30CNC3MAPP	67	30	3
30CNC5MAPP	65	30	5
30CNC7MAPP	63	30	7
40CNC3MAPP	57	40	3
40CNC5MAPP	55	40	5
40CNC7MAPP	53	40	7

3.3.3 Mechanical properties testing

The evaluation of mechanical properties of all composites, including tensile, flexural, and impact properties, was performed according to ASTM D638 (Type IV), ASTM D790-A, and ASTM D256, respectively. A Mark-10 ESM750s motorized test machine (Copiague, NY, USA) with a 2,500-N load cell was used to perform tensile tests at a cross-head speed of 5 mm min^{-1}. The strain of composites was measured by an Epsilon extensometer SN E109112 (Jackson, WY,

USA). At least five specimens from each formulation were tested for tensile properties. Flexural tests were performed using a Mark-10 ESM750s motorized test machine (Copiague, NY, USA) equipped with a 500-N load cell at a cross-head speed of 1.34 mm min^{-1}. Five specimens from each formulation were tested for flexural properties. The notched Izod impact tests were carried out with a Zwick/Roll HIT 25P (Germany) impact tester equipped with a 1 J pendulum for CNC/MAPP/HPP composites. A V-shape notch with a depth of 2.54 mm and a notch angle of 45° was created using a manual Instron CEAST notcher (Norwood, MA, USA) prior to conducting the impact test for all specimens. Ten specimens from each formulation were tested for impact strength (kg m^{-2}). All tests were conducted at room temperature of 23 ± 2 °C with 50 ± 5 % RH.

3.3.4 Water absorption testing

Five impact fractured samples from each formulation were used to measure water gain, thickness swell, and width swell. The average thickness and width measurements were obtained from three points on each sample. All of the specimens were conditioned by oven drying at 105 °C to a constant weight. Afterward, weighing and measuring them to the nearest 0.0001 g and 0.001 mm before immersing them in deionized water at a room temperature of 23 ± 2 °C for a long duration (150 days). At specific time intervals (every day in the first week, one or two-week intervals therafter), the specimens were removed from the water and dried with Kimtech kimwipes, followed by weighing and dimensional measurement, and then was inserted back into the water. The percentages of water gain and thickness and width swell were calculated according to the following equations:

$$\text{Water gain (\%)} = (W_t - W_0)/W_0 \times 100 \qquad (1)$$

$$\text{Thickness swell (\%)} = (T_t - T_0)/T_0 \times 100 \quad (2)$$

$$\text{Width swell (\%)} = (w_t - w_0)/w_0 \times 100 \quad (3)$$

Where W_0, T_0, and w_0 are the initial weight, thickness, and width of the specimens before water immersion, W_t, T_t, and w_t are the weight, thickness, and width after water immersion for specific time intervals, respectively.

Diffusion coefficients (D) for all composites were calculated according to the following model [25,26]:

$$M_t/M_\infty = (4/h) * (D/\pi)^{\frac{1}{2}} * t^{\frac{1}{2}} \quad (4)$$

Where M_t is water gain at immersion time t, M_∞ is the equilibrium water gain (assumed to be the maximum water gain at the end of the experiment (150 days)), h is the sample thickness.

3.3.5 Morphological properties

A Zeiss Evo 50VP scanning electron microscope (SEM) (Oberkochen, Germany) was used to examine the Izod impact-tested cross-section surfaces of all the composites to evaluate the morphological properties. An accelerating voltage of 20 kV was used for the SEM work. The specimen surfaces were sputter-coated with gold for 60 s by a Q150R ES sputter coater (Hatfield, PA, USA) before SEM observation.

3.3.6 Thermal characterization

Differential scanning calorimetry (DSC) analysis was performed using a TA instrument DSC-250 (DE, USA) under a nitrogen atmosphere with the following conditions: 1) heating about 10-15 mg sealed sample from 40 °C to 200 °C, 2) keeping at 200 °C for 2 min to eliminate the

previous thermal history, 3) cooling down to 40 °C, 4) isothermal at 40 °C for 2 min, 5) reheating to 200 °C. Both heating and cooling rates were 10 °C min^{-1}. The cooling and second heating thermograms were analyzed using the TRIOS (TA Instruments, DE, USA) software. At least duplicates were tested for each sample. The crystallinity X_c (%) was calculated using the following equation:

$$X_c\ (\%) = \Delta H_m/(\Delta H_m^0\ w_{HPP}) \times 100\% \qquad (5)$$

Where ΔH_m is the melting enthalpy obtained from the second heating cycle; ΔH_m^0 is the melting enthalpy of HPP with 100% crystallinity extracted from the literature (205 J mol^{-1}) ; [27] and w_{HPP} is the weight ratio of HPP in the composite.

3.3.7 Statistical analysis

One-way ANOVA (analysis of variance) with a 0.05 significance level, followed by Tukey's *post-hoc* tests, was applied to separately analyze the mechanical properties of CNC/HPP composites and water absorption properties of all composites, respectively. The effect of different loadings of SDCNC and MAPP on each mechanical property was analyzed using two-way ANOVA with Tukey's *post-hoc* tests at a 0.05 significance level. The two-factor model was:

$$Y_{ijk} = \mu + \alpha_i + \beta_j + \gamma_{ij} + \varepsilon_{ijk} \sim N(0, \sigma) \qquad (6)$$

Where i = 1, 2; j = 1, 2, 3, 4; k = 1, 2, 3, 4, 5, 6, 7 (tensile properties) or 1, 2, 3, 4, 5 (flexural properties) or 1, 2, 3, 4, 5, 6, 7, 8, 9, 10 (impact properties); Y_{ijk} is the mean value of each mechanical property tested; μ is the population mean value of each mechanical property; α_i and β_j are the effects of SDCNC and MAPP contents on the mechanical properties; γ_{ij} is the

interaction effect between SDCNC and MAPP on the mechanical properties; and ε_{ijk} is the error associated with a normal distribution (N) and standard deviation (σ).

3.4 Results and discussions

3.4.1 Mechanical properties

The effect of various loadings (20, 30, 40, and 50 wt. %) of SDCNC particles on the mechanical properties of the composites was evaluated (Table 3-2). The incorporation of high-stiffness SDCNC resulted in all CNC/HPP composites having greater tensile MOE than neat HPP (1.34 ± 0.03 GPa). The tensile moduli increased as the SDCNC content increased, reaching up to 2.99 ± 0.23 GPa for 50CNC, which was 123% higher than that of neat HPP. On the contrary, the tensile strength and tensile strain at the yield point decreased monotonically with increasing SDCNC content compared to neat HPP (Table 3-2). The decrease was ascribed to the incompatibility between hydrophilic SDCNC particles and hydrophobic HPP matrix without a compatibilizer, generating separated interfacial space (Figure 3-1A-D) and an ineffective stress transfer. The addition of rigid SDCNC particles could restrict the mobility of polymer chains and reduce the ductility of the composites. [28,29]

The flexural MOE of CNC/HPP composite steadily increased with rising the SDCNC content, reaching up to 2.87 ± 0.08 GPa for 50CNC, approximately 117% higher than that of neat HPP. This trend aligns well with the change in tensile MOE. Flexural strength, reported as the stress at yield point for 30CNC, 40CNC, and 50CNC and the stress at 5 % strain for HPP and 20CNC (no yield or break before 5 % strain according to the ASTM D790-A), demonstrated a

complex relationship. A significant increase in flexural strength occurred for 20CNC and 30CNC, followed by a significant decrease for 40CNC and 50CNC. The higher filler content led to closer spacing between SDCNC particles, facilitating to form large aggregates and inducing extra stress concentration points in the composite, impeding the stress transfer. Consequently, the flexural strength decreased at greater filler loading levels.

Table 3-2. The mechanical properties of CNC/HPP composites.

Sample	Tensile Properties			Flexural Properties		Impact Strength (kJ m^{-2})
	MOE (GPa)	Strength (MPa)	Strain (%)	MOE (GPa)	Strength[c] (MPa)	
HPP	1.34±0.03[a] E[b]	30.2±0.2 A	10.3±0.6 A	1.32±0.02 E	40.7±0.5 B	1.59±0.12 B
20CNC	2.05±0.09 D	26.1±0.6 B	5.2±0.5 B	1.72±0.04 D	42.9±0.9 A	1.85±0.15 A
30CNC	2.38±0.10 C	22.6±0.3 C	3.9±0.3 C	2.04±0.02 C	42.4±0.3 A	1.95±0.21 A
40CNC	2.68±0.12 B	20.3±0.4 D	2.8±0.1 D	2.46±0.02 B	39.5±0.5 C	1.48±0.25 B
50CNC	2.99±0.23 A	17.7±0.5 E	2.2±0.3 E	2.87±0.08 A	35.0±0.3 D	1.39±0.10 B

[a]Mean value and standard deviation.

[b]For each column, different letters represent the significant difference ($p<0.05$).

[c]Flexural strength values were reported at a 5 % strain limit for HPP and 20CNC and at yield points for 30CNC, 40CNC, and 50CNC.

The impact strength of CNC/HPP composites increased initially with 20 and 30 wt.% of SDCNC, peaking at 1.95±0.21 kJ m^{-2} for 30CNC (20% higher than that of neat HPP), then decreased to 1.48±0.25 and 1.39±0.10 kJ m^{-2} for 40CNC and 50CNC, showing no statistically significant differences from the neat HPP based on the statistical analysis (Table 3-2). The physical adhesion based on the mechanical interlocking between the SDCNC particles and the HPP matrix, caused by the irregular shapes of SDCNC, was the reason for the increased impact strength. This

mechanical interlocking failure mode of the polymer strands with stretched filaments can be clearly seen in (Figure 3-1A-D**.** The longer and more filaments and the rougher surfaces of 20CNC and 30CNC composites indicated that higher energy was required for the impact test fracture (Figure 3-1A-B). However, at higher SDCNC levels (40CNC and 50CNC), more particles embedded in the HPP matrix, large agglomerates of SDCNC particles without effective contact with the matrix formed, interrupting the integrity between SDCNC particles and the HPP matrix caused by the mechanical interlocking adhesion. Simultaneously, the fracture surface (Figure 3-1C-D) may demonstrate the fracture paths going through spaces between SDCNC particles without involving the polymer matrix during the impact test. The SDCNC particles are spray-dried, and the adhesion between the particles is weak. Hence, the impact strength decreased at higher SDCNC loading levels that increase the fracture probability at the interfaces of the SDCNC particles.

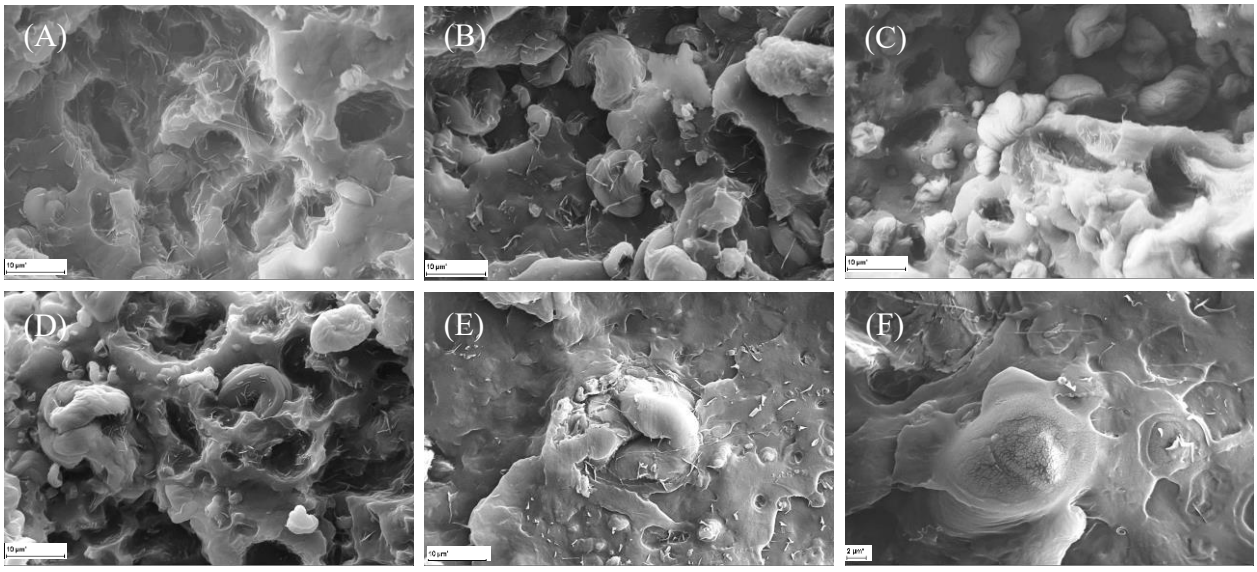

Figure 3-1 The morphological properties of all composites: 20CNC (A), 30CNC (B), 40CNC (C), 50CNC (D), and 30CNC5MAPP (E-F).

Table 3-3. Two-way ANOVA on mechanical properties of CNC/MAPP/HPP composites

Source	Degree of freedom	*P* value					
		Tensile Properties			Flexural Properties		Impact Strength
		MOE	Strength	Strain	MOE	Strength	
CNC	1	1.34E-13	7.77E-10	1.47E-7	1.63E-27	2.39E-12	4.20E-4
MAPP	3	0.1984	3.10E-36	9.15E-13	9.73E-17	4.00E-32	9.26E-37
CNC*MAPP	3	0.2083	2.21E-6	0.0731	1.17E-5	1.78E-14	5.25E-6
Model	7	1.42E-10	1.87E-34	1.91E-12	9.85E-26	6.81E-31	3.15E-35

Table 3-4 The mechanical properties of all CNC/MAPP/HPP composites.

Composites	Tensile Properties			Flexural Properties		Impact Strength (kJ/m^2)
	MOE (GPa)	Strength (MPa)	Strain (%)	MOE (GPa)	Strength[c] (MPa)	
30CNC	2.38±0.10[a] B[b]	22.6±0.3 C	3.9±0.3 C	2.04±0.02 D	42.4±0.3 D	1.95±0.21 B
30CNC3MAPP	2.20±0.05 B	32.4±0.1 A	5.3±0.1 A	1.87±0.02 E	51.8±0.6 C	2.72±0.10 A
30CNC5MAPP	2.28±0.07 B	32.5±0.2 A	5.2±0.4 A	1.91±0.03 E	52.8±0.7 C	2.81±0.09 A
30CNC7MAPP	2.30±0.04 B	32.4±0.5 A	5.1±0.4 AB	1.91±0.03 E	53.0±0.9 C	2.73±0.09 A
40CNC	2.68±0.12 A	20.3±0.4 D	2.8±0.1 D	2.46±0.02 A	39.5±0.5 E	1.48±0.25 C
40CNC3MAPP	2.68±0.06 A	32.1±0.2 AB	4.5±0.3 BC	2.25±0.03 B	57.3±0.4 A	2.68±0.10 A
40CNC5MAPP	2.69±0.06 A	31.4±0.4 B	4.8±0.4 AB	2.19±0.04 C	55.9±0.9 B	2.82±0.14 A
40CNC7MAPP	2.69±0.04 A	32.0±0.4 AB	4.6±0.4 AB	2.21±0.03 BC	56.4±0.5 AB	2.72±0.16 A

[a]Mean value and standard deviation.

[b]For each column, different letters represent the significant difference ($p<0.05$).

[c]Flexural strength was reported at yield point for 30CNC and 40CNC and at 5% strain limit for others.

The flexural and impact strength of 40CNC is significantly lower than those of 30CNC and 20CNC, which are not substantially different from each other, implying a dramatic internal structure in CNC/HPP composites when the SDCNC loading changes from 30 to 40 wt.%. The percolation network of SDCNC particles was possibly established between 30 – 40 wt.%. Thus, composites with 30 and 40 wt. % SDCNC were selected to study the effect of MAPP, which was used to enhance the compatibility between SDCNC particles and the HPP matrix.

Two-way ANOVA results on the mechanical properties of the CNC/MAPP/HPP composites showed a significant interactive effect between the SDCNC and MAPP content on all mechanical properties, except for tensile MOE and strain properties (Table 3-3). Tensile strength and strain increased significantly when introducing MAPP as a compatibilizer in the composites. For example, 30CNC3MAPP and 40CNC3MAPP exhibited a 36 % and 61 % increase in tensile strain and a 43 % and 58 % improvement in tensile strength compared to the corresponding CNC/HPP composites (Table 3-4). In addition, the tensile strength of CNC/MAPP/HPP composites with 30 wt. % SDCNC was also approximately 7 % higher than that of neat HPP (30.2±0.2 MPa). The increment was ascribed to the enhanced compatibility between the SDCNC particles and HPP matrix, as shown in Figure 3-1E-F. Compared to the 30CNC composite (Figure 3-1B), no separated interfaces or gaps between SDCNC particles and matrix were observed and all SDCNC particles were covered by polymer (Figure 3-1E-F), increasing the whole composite's continuity and promoting the effective stress transfer from matrix to SDCNC particles. These results indicated that MAPP served as an excellent compatibilizer for CNC/HPP composite by

establishing improved interfacial adhesion. Statistically, there are no significant differences in the tensile strength and strain under the same SDCNC loading with various MAPP levels (Table 3-4). In the case of tensile MOE, the SDCNC particle loading level had a substantial effect, while the MAPP content had no significant impact on it (Table 3-3). This can be explained by that MOE is unaffected by the particle/matrix interfacial adhesion quality in particle-polymer composite systems. [11]

A similar trend was observed regarding flexural strength of the composites with MAPP (Table 3-4). Flexural strength was significantly improved up to 53.0±0.9 MPa (30CNC7MAPP) and 57.3±0.4 MPa (40CNC3MAPP), representing 25 % and 45 % higher than the corresponding values of 30CNC and 40CNC. Flexural MOE significantly decreased after adding MAPP (Table 3-4) due to MAPP's higher melt flow index (115 g 10 min^{-1}) compared to HPP (20 g 10 min^{-1}). Generally, a lower molecular weight polymer has lower stiffness. [29,30] Based on the rule of mixtures, the CNC/MAPP/HPP composites have lower flexural MOE. At the 3, 5, and 7 wt.% MAPP loading levels, the composites performed similar flexural properties.

The addition of MAPP significantly increased the impact strength (Table 3-4). The impact strength of 30CNC5MAPP and 40CNC5MAPP are 2.81±0.09 and 2.82±0.14 kJ m^{-2}, representing a 44% and 91% improvement over 30CNC and 40CNC and a 59% enhancement over neat HPP (1.77±0.20 kJ m^{-2}). This dramatic increment is associated with the improved compatibility between the matrix and the SDCNC particles, visible in SEM micrographs (Figure 3-1E-F). The introduction of MAPP resulted in a new layer of polymer coating on the SDCNC particle surfaces,

achieving polymer fracture and increasing toughness, which imply a successful interaction between SDCNC, MAPP, and HPP. The possible interfacial interaction can be interpreted by the creation of covalent (ester linkages between SDCNC and MAPP) and hydrogen (the interaction between anhydride groups and hydroxyl groups of SDCNC) bonds. [31,32] The similar chemical structure of the PP moiety of MAPP and HPP matrix permits good miscibility and strengthens the interfacial adhesion of the composite. The improved interfacial adhesion, in turn, contributes to mechanical property enhancement. At the same SDCNC loading level, no significant difference in impact strength was observed for the CNC/MAPP/HPP composites with varying MAPP contents.

3.4.2 Water absorption testing

Water absorption testing was performed to evaluate the distribution of SDCNC particles in the HPP matrix and to explore the possible change in the internal structure of CNC/HPP and CNC/MAPP/HPP composites. The percentage of the water gain for all composites during immersion into DI water was plotted against the square root of time in Figure 3-2. The percentages of the water gain and the thickness and width swell were calculated from five replicates, diffusion coefficients based on the initial slope of this curve at the early stage (25 days) were also calculated, as shown in Table 3-5 and Table 3-6.

The results indicated that the neat HPP has an excellent water barrier property. The water gain increased as the SDCNC particle loading level in the composite increased because of its hydrophilic nature. Water molecules mainly diffused into the SDCNC particles because of their

hygroscopic nature, swelling the particles, and then migrated within the composites through SDCNC particles or along SDCNC-HPP interfaces. Theoretically, increasing SDCNC particle loading levels in the composite is expected to result in a proportional increment in equilibrium water gain due to the hydrophilic nature of SDCNC and the expansion of interfacial areas between SDCNC and HPP. This linear relationship can be observed from the equilibrium water gains of 20CNC and 30CNC (Table 3-5), i.e., there is a direct proportional relationship between the SDCNC loading and the equilibrium water gain. The water gain to SDCNC loading ratio is same for 20CNC and 30CNC (0.066±0.001). However, at higher SDCNC loading, the ratio is much higher (0.080±0.002 and 0.193±0.003 for 40CNC and 50CNC, respectively) (Table 3-5). This observation indicated that: 1) there is no considerable change in the SDCNC network or distribution in 20CNC and 30CNC; 2) the SDCNC networks or distributions in 40CNC and 50CNC differ dramatically from 20CNC, 30CNC, and each other; and 3) the SDCNC percolation threshold is between 30 – 40 wt.%.

The proposed mechanism of water absorption, based on the suggested percolation theory, is illustrated in Figure 3-3. SDCNC particles were uniformly distributed in HPP, completely encapsulated by the matrix, and separated from each other in 20CNC (Figure 3-3A). The major water absorption pathway was the diffusion of water molecules from the specimen surface (either through SDCNC particles or HPP) and the interface between surface SDCNC and HPP to another phase of SDCNC or HPP inside. The diffusion rate for pure HPP was extremely low, with a diffusion coefficient of 4.81E-07mm^2 h^{-1}, while 20CNC exhibited a notable 3000-fold increase. It

revealed that SDCNC particles had a remarkable potential to facilitate the absorption of water molecules through hydrogen bonding. [20] The diffusion coefficient of 30CNC is 160% higher than that of 20CNC. With the same ratios of water gain to SDCNC loadings, the change in the diffusion coefficient is mainly due to the increased SDCNC loading. A higher water diffusion coefficient of 30CNC may indicate local SDCNC particle agglomerates may be present, as proposed in Figure 3-3B. In 30CNC, individual and locally agglomerated SDCNC particles were still encapsulated by HPP. Consequently, the matrix, the dispersed SDCNC particles and agglomerates still predominantly governed water molecule diffusion. As SDCNC loading further increase, the water diffusion coefficient of 40CNC increased by about seven times compared to 20CNC, which is assumed to be two times if there were no internal structure changes of SDCNC particle distribution. A proposed integrated network structure (percolation) of SDCNC particles is formed inside 40CNC. At this point, the matrix failed to encapsulate all SDCNC particles separately, and water molecules can easily be transported continuously between SDCNC particles throughout the composite structure. Simultaneously, it is proposed that only limited numbers of percolation networks were established in 40CNC (Figure 3-3C). Once more SDCNC percolated networks were established in 50CNC (Figure 3-3D), the water diffusion coefficient increased approximately 60 times compared to 20CNC. The multiple percolated SDCNC networks promote water molecules to move from different directions, enabling faster and more efficient diffusion of water molecules through the composites. The high-density hydroxyl groups of SDCNC particles facilitate hydrogen

bonding interactions with adjacent water molecules, allowing for the easy migration of water molecules along the SDCNC percolation networks.

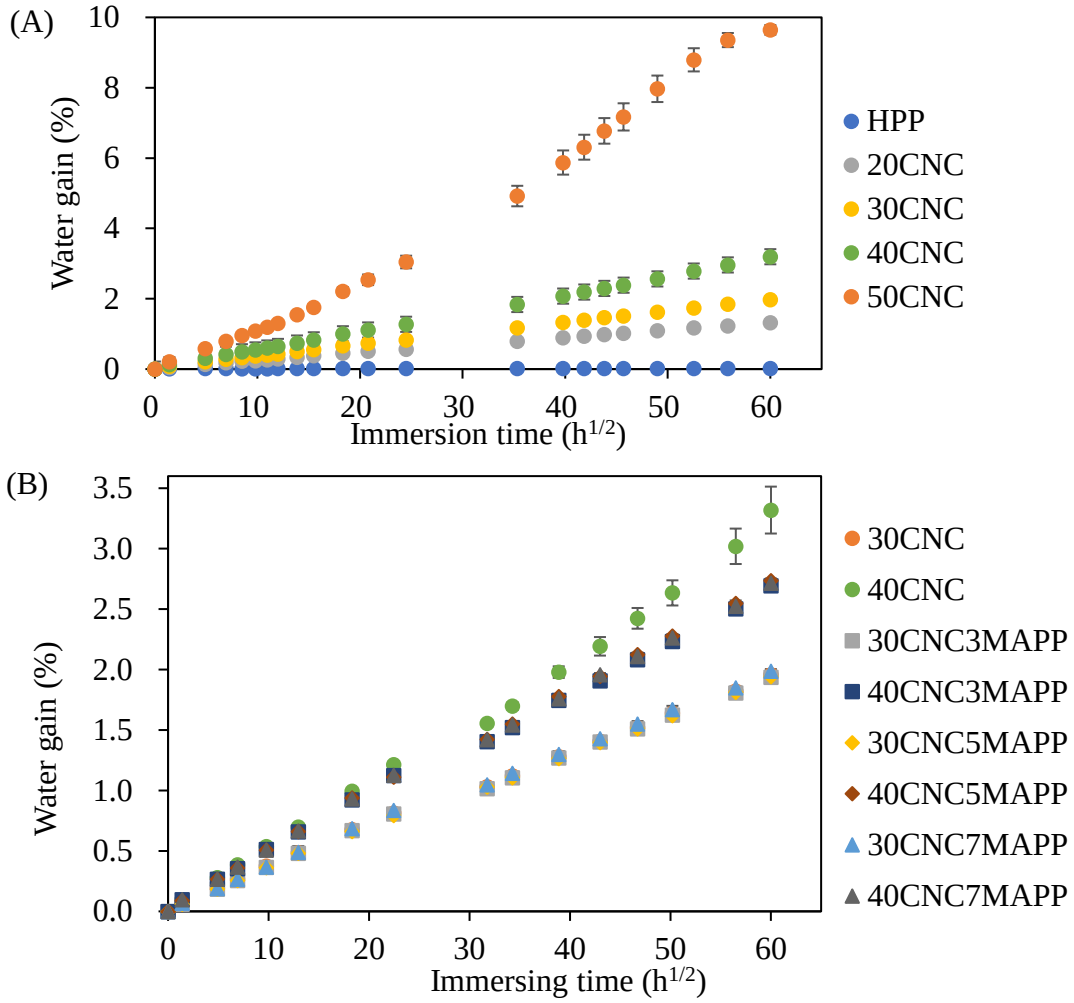

Figure 3-2 Water gain curves for CNC/HPP composites (A) and CNC/MAPP/HPP composites (B).

With the presence of MAPP in 30CNC, the water gain and diffusion coefficient changed slightly (Table 3-6 and Figure 3-2B). The chemical bonding between SDCNC and MAPP subtly changed the interaction between SDCNC particles and water molecules, and decreased the

interfacial space in the composites, leading to a change in water gain. In the case of 30CNC, the effect of MAPP was applied to individual SDCNC particles or local agglomerates, and the impact was limited due to the dispersion and distribution of the SDCNC particles in the matrix. For CNC/MAPP/HPP composite at 40 wt.% SDCNC loadings, the water gain decreased significantly (> 14%) with slight variations at 3, 5, and 7 wt.% MAPP loading (Figure 3-2B and Table 3-6). The water diffusion coefficient also decreased notably. The effect of MAPP on the water gain of the composite with the SDCNC percolation networks is significantly changed by the reduced interfacial space and the interaction between MAPP and the SDCNC particles.

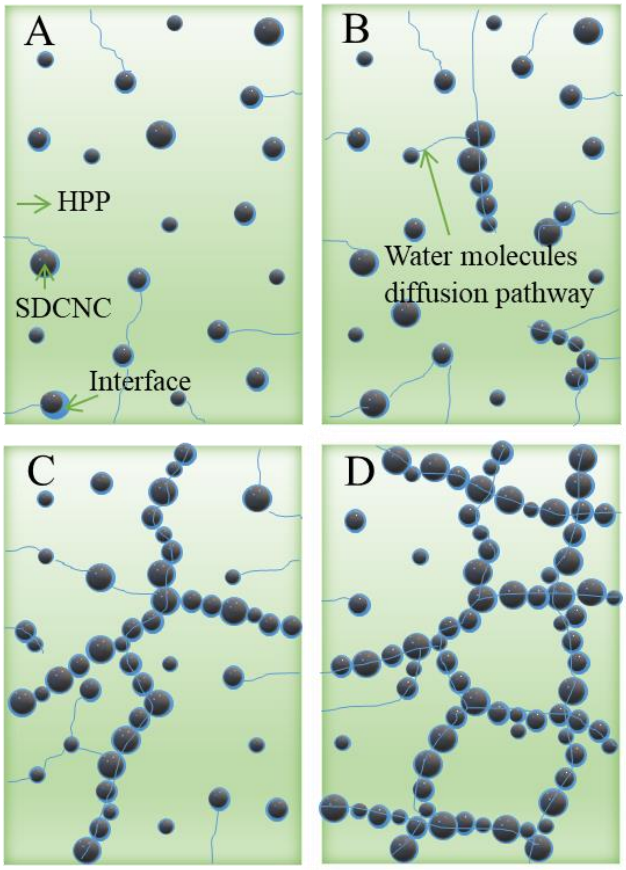

Figure 3-3 The proposed mechanism of water absorption for 20CNC (A), 30CNC (B), 40CNC (C), 50CNC (D).

Another possible reason for the decreased water gain is the effective interaction of MAPP and SDCNC, improving SDCNC particles dispersion and distribution and reducing the probabilities to form the SDCNC percolation networks.

The dimensional stability of the composite was influenced by the swelling of SDCNC particles after absorbing water. The thickness and width swell of all CNC/HPP and

CNC/MAPP/HPP composites performed similarly to the water gain of the composites. Non-significant difference in dimensional swelling between 20CNC and 30CNC indicated the minimized SDCNC network structure change. Higher SDCNC loadings led to significant increase in dimensional swelling (Table 3-5) due to the formed percolation network. However, the overall dimensional change is relatively low (approx. 1%) compared with the wood flours reinforced HPP composites at the same 30 wt. % loading, which indicated the SDCNC particles had a limited impact on the water resistance of HPP composites. [33] The highly impermeable crystalline structure of SDCNC acts as a water barrier and provides a tortuous path for the water molecule diffusion. [34]

Table 3-5. Water absorption properties of CNC/HPP composites after water immersion for 150 days.

Composites	Water gain (%)	Water gain to SDCNC loading ratio	Diffusion coefficient ($mm^2 h^{-1}$)	Thickness swell (%)	Width swell (%)
HPP	0.02±0.01[a] E[b]	-	4.09E-07	0.27±0.05 D	0.07±0.05 D
20CNC	1.32±0.02 D	0.066	1.35E-03	0.86±0.11 C	0.39±0.04 C
30CNC	1.97±0.01 C	0.066	3.59E-03	1.09±0.18 C	0.49±0.04 C
40CNC	3.19±0.01 B	0.080	1.04E-02	1.88±0.22 B	0.81±0.10 B
50CNC	9.64±0.14 A	0.193	8.73E-02	3.84±0.17 A	2.99±0.12 A

[a]Mean value and standard deviation.

[b]For each parameter, different letters represent the significant difference ($p<0.05$).

Table 3-6 Water absorption properties of CNC/MAPP/HPP composites after water immersion for 150 days.

Composites	Water gain (%)	Diffusion coefficient ($mm^2\ h^{-1}$)	Thickness swell (%)	Width swell (%)
30CNC[a]	1.97±0.01[b] A[c]	3.59E-03	1.09±0.18 A	0.49±0.04 A
30CNC3MAPP	1.94±0.02 B	3.71E-03	1.03±0.02 A	0.39±0.02 B
30CNC5MAPP	1.94±0.01 B	3.65E-03	1.03±0.03 A	0.42±0.02 B
30CNC7MAPP	1.99±0.02 A	3.97E-03	1.04±0.05 A	0.40±0.01 B
40CNC	3.19±0.01 A	1.04E-02	1.88±0.22 A	0.81±0.10 A
40CNC3MAPP	2.69±0.01 B	8.44E-03	1.52±0.05 B	0.62±0.02 B
40CNC5MAPP	2.74±0.02 B	8.52E-03	1.59±0.05 B	0.65±0.01 B
40CNC7MAPP	2.72±0.02 B	8.59E-03	1.55±0.04 B	0.61±0.02 B

[a]30CNC and 40CNC composites with different content of MAPP were analyzed separately.

[b]Mean value and standard deviation.

[c]For each parameter, different letters represent the significant difference ($p<0.05$).

3.4.3 Thermal characterization

The crystallization and melting behaviors of all the composites were evaluated by DSC, and the peak temperatures for crystallization and melting are summarized in Table 3-7. The DSC thermograms of the crystallization process are shown in Figure 3-4. For the CNC/HPP composites, the crystallization exothermal curves shifted toward higher temperatures after adding the SDCNC particles (Figure 3-4A). The HPP crystallization peak temperature (T_c) is 112.5±0.1 °C. Adding 20 wt.% SDCNC particles in the composite increased the T_c of HPP to 122.1±0.3 °C. This increment is caused by the nucleation function of the cellulose surface, forming a well-known transcrystalline layer around the SDCNC particles .[35,36] Adding 30 wt.% SDCNC further increased

the HPP T_c to 124.5±0.2 °C, a minor increase compared with 20CNC composite. This observation indicated that more cellulose HPP interfacial area was created for 30CNC than that for 20CNC, further increasing the nucleation function of the cellulose surface. However, further increase of the SDCNC loadings did not increase T_c of HPP in 40CNC (124.4±0.6 °C) and 50CNC (124.8±1.3 °C). The relationship between the T_c and the SDCNC loading levels is shown in Figure 3-4B. These results indicated that: 1) the SDCNC particles acted as an effective nucleating agent in the HPP matrix, [10,31,37] inducing the formation of additional nucleation sites to facilitate the crystallization of HPP at a higher temperature; 2) the T_c of HPP changed with SDCNC loading level up to the percolation threshold due to surface nucleation function of cellulose; 3) the amounts of the SDCNC and HPP interface in 40CNC and 50CNC were similar to that in 30CNC which is slightly greater than that in 20CNC; and 4) 30 wt.% SDCNC particles in the HPP saturated the nucleation function of the cellulose surface for the HPP. In other words, 30 wt. % SDCNC particles in the HPP matrix provided a maximum nucleation function, and adding more SDCNC particles barely affected the crystallization process of HPP. The crystallization study can be correlated with the mechanical property and water absorption results to further refine the percolation threshold of the SDCNC in HPP, which is around 30 wt.%.

The melting peak temperatures (T_m) of all the CNC/HPP composites (Table 3-7 and Figure 3-5A), were observed at around 162 °C, corresponding to the α-phase crystallite of HPP. [38,39] A notable shoulder at approximately 155 °C was observed during the second melting process for composites with the SDCNC loading level at 30 wt.% or above (Figure 3-5A). The lower melting

temperature was identified as the β-phase HPP crystallite, [38] which indicated that the SDCNC particles in HPP matrix promoted the formation of β-phase crystallite of HPP. The appearance of the β-phase crystallite can partially explain the improved impact strength of composites since it has better impact resistance than the α-phase HPP. [38,40,41] The melting enthalpy and crystallinity of the HPP were also plotted against the SDCNC loading levels, and a linear relationship was observed (Figure 3-5B-C). The crystallinity (X_c) of the HPP increased from 41.3±0.9 % to 45.1±0.9 % with the incorporation of 50 wt. % SDCNC within the HPP matrix (Table 3-7). Similarly, the crystallization enthalpies were also observed to be linearly decreasing with the increasing SDCNC loadings (Figure 3-5B).

Including MAPP in CNC/MAPP/HPP composites decreased T_c (Table 3-7 and Figure 3-6). Replacing the HPP with 3 wt.% of MAPP decreased the T_c from 124.5±0.2 and 124.4±0.6 for 30CNC and 40CNC to 120.1±0.3 and 120.8±0.7 °C, respectively. The addition of MAPP at 5 and 7 wt.% slightly decreased the T_c further (Table 3-7). MAPP limited the nucleation function of SDCNC on the HPP, possibly obstructing the formation and growth of HPP crystallite on SDCNC surface. The chemical bonding between MAPP and SDCNC covered the SDCNC particle surface with a different interphase layer, reducing the number of nucleating sites supported by SDCNC and delaying the crystallization process. However, the T_c of HPP in the CNC/MAPP/HPP composites are still higher than that of neat HPP. The change of the SDCNC nucleation function by MAPP may not be able to completely diminish the nucleating effect of the SDCNC particles. The other reason is that introducing MAPP may result in a different nucleation mechanism,

changing the crystallization peak temperatures. The effects of the MAPP on the composite melting behaviors and degrees of crystallinity were also studied, and the results are included in Table 3-7. No notable changes in melting and crystallinity were observed.

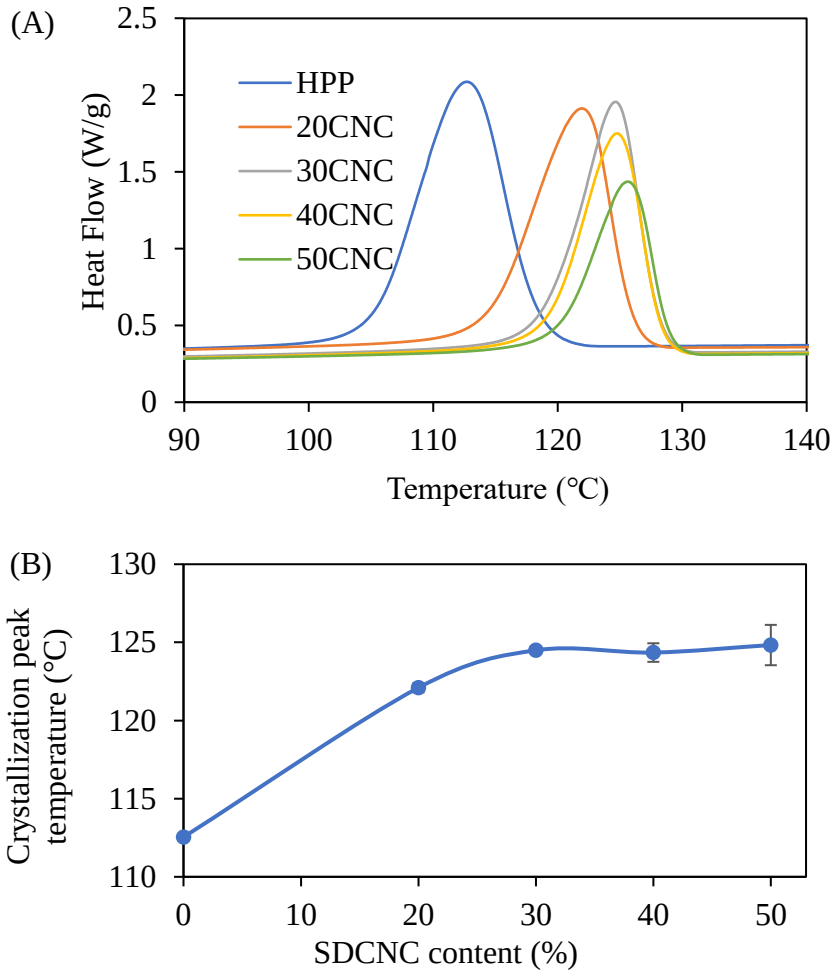

Figure 3-4 The crystallization exothermal curves of CNC/HPP composites (A). The relationship between crystallization peak temperature and the SDCNC loadings (B).

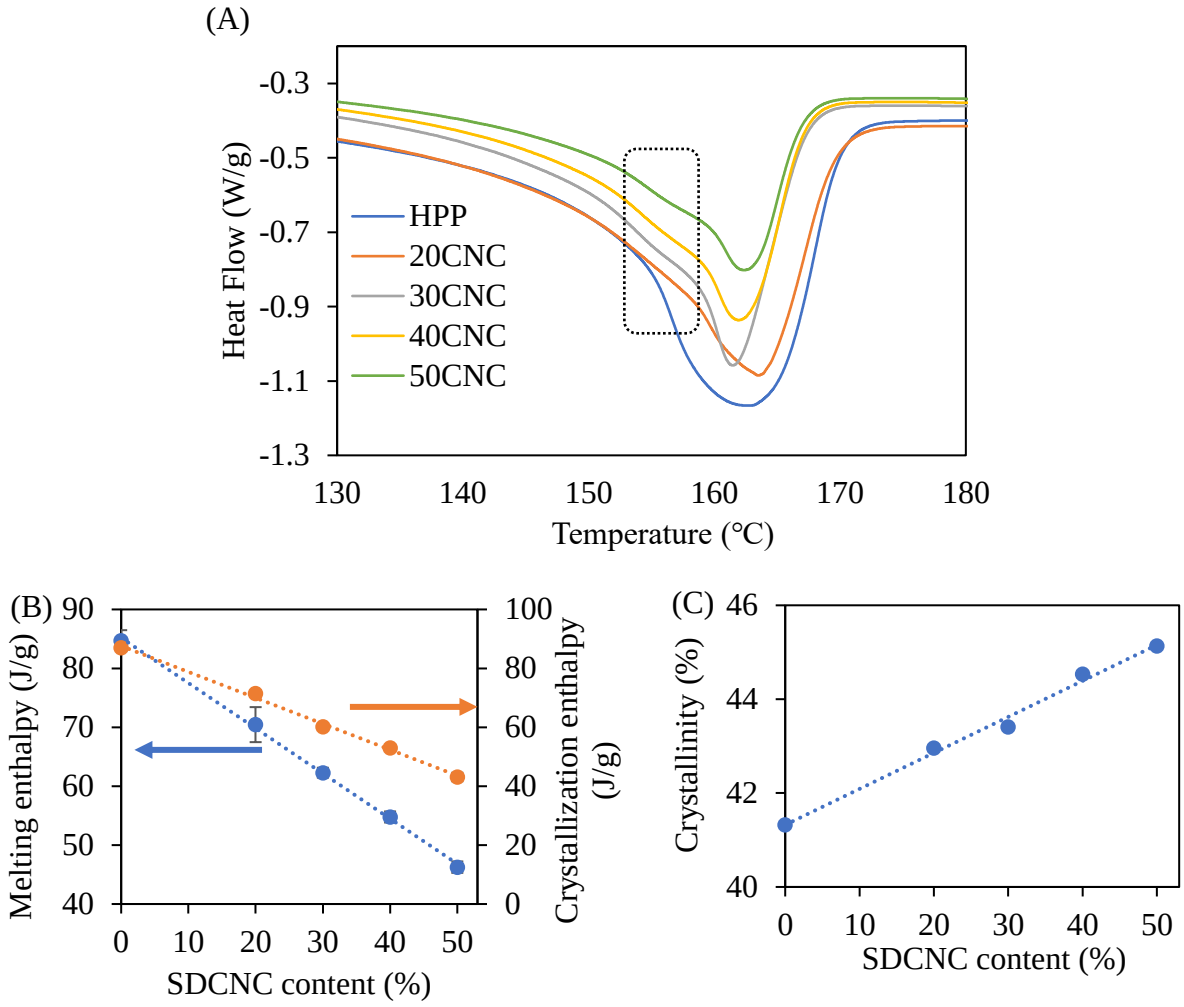

Figure 3-5 The melting endothermal curves of CNC/HPP composites (A), and the relationship between melting and crystallization enthalpy (B) and crystallinity (C) and SDCNC content.

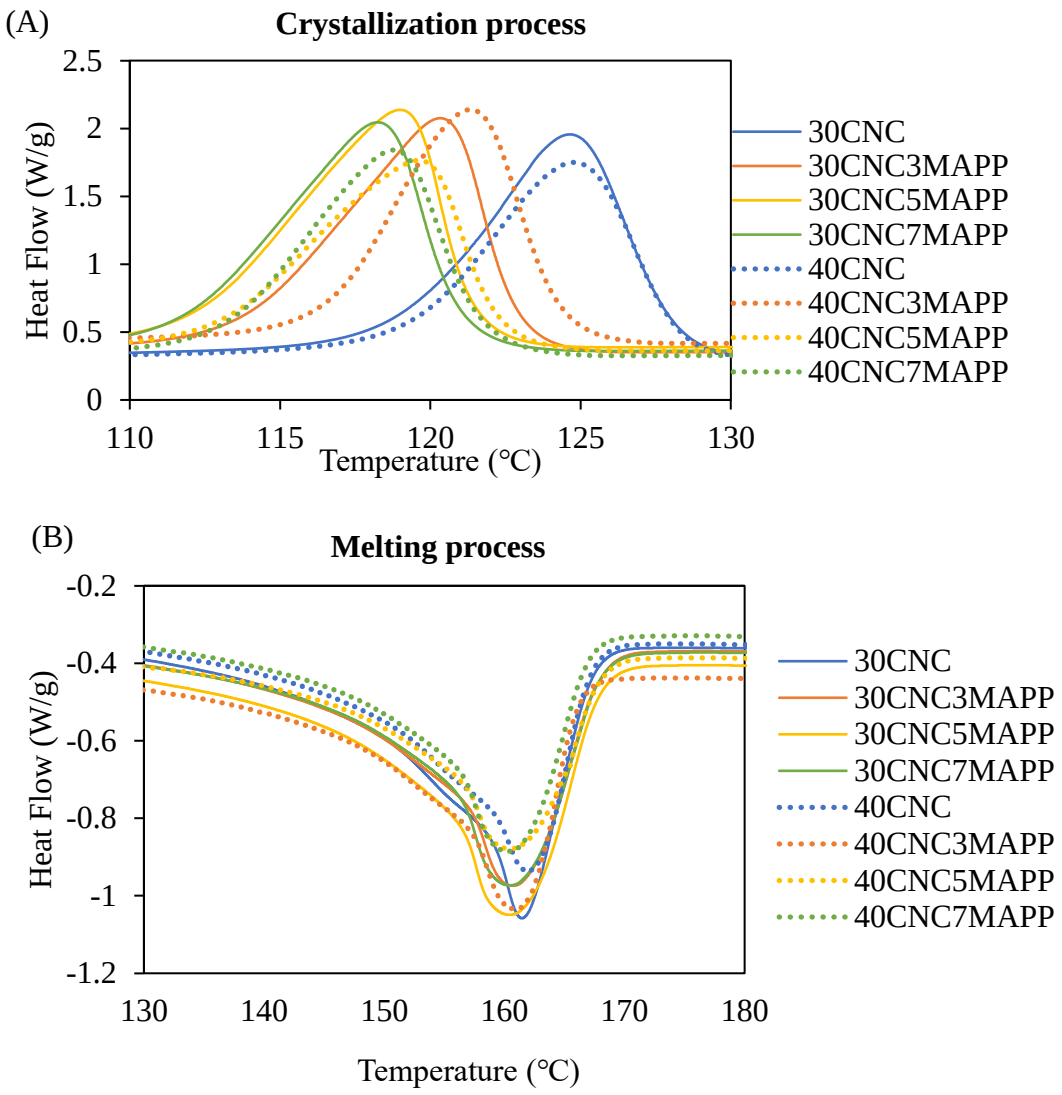

Figure 3-6 The crystallization exothermal (A) and melting endothermal (B) curves of CNC/MAPP/HPP composites.

Table 3-7. The thermal characterizations of all composites.

Samples	Melting process		Crystallization process		X_c (%)
	ΔH_m (J/g)	T_m (°C)	ΔH_c (J/g)	T_c (°C)	
HPP	84.7±1.8	161.6±0.9	87.0±1.1	112.5±0.1	41.3±0.9
20CNC	69.0±2.8	161.9±0.3	77.4±0.6	122.1±0.3	43.0±1.8
30CNC	62.3±0.8	161.3±0.4	60.5±0.6	124.5±0.2	43.4±0.6
40CNC	54.8±0.9	162.6±1.1	53.0±1.0	124.4±0.6	44.5±0.8
50CNC	46.3±1.0	162.0±0.4	43.1±1.5	124.8±1.3	45.1±0.9
30CNC3MAPP	62.3±1.9	161.1±0.7	63.4±0.6	120.1±0.3	43.4±1.3
30CNC5MAPP	64.4±0.6	160.8±0.4	65.8±0.1	118.8±0.2	44.9±0.4
30CNC7MAPP	62.0±0.5	160.9±0.8	63.0±0.1	118.1±0.2	43.2±0.4
40CNC3MAPP	54.7±0.5	161.1±0.3	55.2±1.9	120.8±0.7	44.5±0.4
40CNC5MAPP	53.5±1.6	160.9±0.7	53.0±0.7	119.4±0.4	43.5±1.3
40CNC7MAPP	55.0±0.2	160.7±0.5	53.0±0.1	118.6±0.2	44.7±0.2

3.5 Conclusions

The study explored the percolation threshold of the SDCNC particles in HPP composites and assessed its influence on the mechanical, morphological, and thermal properties of the CNC/HPP composites. Water absorption measurement of the composites, used as a novel method, helped predict the percolation threshold and the internal structure changes of the composites. Additionally, the effect of MAPP as a compatibilizer (3, 5, and 7 wt.%) on the composite percolation network, mechanical, and thermal properties was investigated.

The mechanical properties of the CNC/HPP composites showed that incorporating SDCNC particles improved tensile and flexural MOE significantly by up to 123 % and 117 % at the highest loading levels compared to the neat HPP. Notably, impact strength significantly increased by 20% at 30 wt. % SDCNC, followed by a subsequent decrease at higher loadings, indicating that percolation networks were formed probably between 30 – 40 wt. % of the SDCNC particles. The results of water absorption measurements confirmed the percolation threshold value of the SDCNC particles in HPP composites, as the water gain changed dramatically above 30 wt. % SDCNC loading, indicating a notable change in the internal structure or distribution of the SDCNC particles in the composites. The hypothesis that water absorption behaviors of the composites can be used to identify the particle percolation threshold is confirmed. Simultaneously, the hypothesis that mechanical properties decreased significantly above the SDCNC percolation threshold is confirmed by the impact strength change. Moreover, SDCNC particles acted as nucleating agents,

elevating crystallization peak temperature and crystallinity. Above the SDCNC percolation threshold, the crystallization behavior of HPP in the CNC/HPP composites remained relatively unchanged due to the saturated nucleation function provided by 30 wt. % SDCNC particles.

The addition of MAPP had a limited influence on the internal structure of the 30CNC composite but a more significant impact on the 40CNC composites based on the moisture absorption measurement. At the 40 wt.% SDCNC loading level, which is above the percolation threshold, the tensile strength, tensile strain, flexural strength, and impact strength of the CNC/MAPP/HPP composites were significantly enhanced compared to the corresponding CNC/HPP composites, increasing by up to 58, 61%, 45%, and 91%, respectively. Therefore, the third hypothesis about the effect of MAPP is also confirmed. These improvements were ascribed to the effective interfacial adhesion between the SDCNC particles and the matrix. Various MAPP contents in composites provided similar mechanical properties. However, the introduction of MAPP depressed the crystallization process of HPP in the CNC/MAPP/HPP composites, restricting the nucleation function of SDCNC and hindering the formation and growth of the crystallites of HPP on the SDCNC surfaces.

3.6 References

1. Hao WS, Wang MZ, Zhou FS, et al. A review on nanocellulose as a lightweight filler of polyolefin composites. *Carbohyd Polym*. Sep 1 2020;243. doi:https://doi.org/10.1016/j.carbpol.2020.116466

2. Spoljaric S, Genovese A, Shanks RA. Polypropylene-microcrystalline cellulose composites with enhanced compatibility and properties. *Compos Part a-Appl S*. Jul 2009;40(6-7):791-799. doi:https://doi.org/10.1016/j.compositesa.2009.03.011

3. Singh MK, Mohanty AK, Misra M. Upcycling of waste polyolefins in natural fiber and sustainable filler-based biocomposites: A study on recent developments and future perspectives. *Compos Part B-Eng*. Aug 15 2023;263doi:https://doi.org/10.1016/j.compositesb.2023.110852

4. Chafidz A, Ali MAH, Elleithy R. Morphological, thermal, rheological, and mechanical properties of polypropylene-nanoclay composites prepared from masterbatch in a twin screw extruder. *J Mater Sci*. Sep 2011;46(18):6075-6086. doi:https://doi.org/10.1007/s10853-011-5570-0

5. Fu SY, Lauke B, Mäder E, Yue CY, Hu X. Tensile properties of short-glass-fiber- and short-carbon-fiber-reinforced polypropylene composites. *Compos Part a-Appl S*. 2000;31(10):1117-1125. doi:https://doi.org/10.1016/S1359-835X(00)00068-3

6. Ghoshal S, Wang PH, Gulgunje P, Verghese N, Kumar S. High impact strength polypropylene containing carbon nanotubes. *Polymer*. Sep 25 2016;100:259-274. doi:https://doi.org/10.1016/j.polymer.2016.07.069

7. Peng YC, Musah M, Via B, Wang XQ. Calcium Carbonate Particles Filled Homopolymer Polypropylene at Different Loading Levels: Mechanical Properties Characterization and Materials Failure Analysis. *J Compos Sci*. Nov 2021;5(11)doi:https://doi.org/10.3390/jcs5110302

8. Premalal HGB, Ismail H, Baharin A. Comparison of the mechanical properties of rice husk powder filled polypropylene composites with talc filled polypropylene composites. *Polym Test*. Oct 2002;21(7):833-839. doi:https://doi.org/10.1016/S0142-9418(02)00018-1

9. Shajari S, Arjmand M, Pawar SP, Sundararaj U, Sudak LJ. Synergistic effect of hybrid stainless steel fiber and carbon nanotube on mechanical properties and electromagnetic interference shielding of polypropylene nanocomposites. *Compos Part B-Eng*. May 15 2019;165:662-670. doi:https://doi.org/10.1016/j.compositesb.2019.02.044

10. Sojoudiasli H, Heuzey MC, Carreau PJ. Mechanical and morphological properties of cellulose nanocrystal-polypropylene composites. *Polym Composite*. Oct 2018;39(10):3605-3617. doi:https://doi.org/10.1002/pc.24383

11. Fu SY, Feng XQ, Lauke B, Mai YW. Effects of particle size, particle/matrix interface adhesion and particle loading on mechanical properties of particulate-polymer composites. *Compos Part B-Eng*. Sep 2008;39(6):933-961. doi:https://doi.org/10.1016/j.compositesb.2008.01.002

12. Huang TX, Kwan I, Li KD, Ek M. Effect of cellulose oxalate as cellulosic reinforcement in ternary composites of polypropylene/maleated polypropylene/cellulose. *Compos Part a-Appl S*. Jul 2020;134doi:https://doi.org/10.1016/j.compositesa.2020.105894

13. Agarwal J, Mohanty S, Nayak SK. Valorization of pineapple peel waste and sisal fiber: Study of cellulose nanocrystals on polypropylene nanocomposites. *J Appl Polym Sci*. Nov 10 2020;137(42)doi: https://doi.org/10.1002/app.49291

14. Wu Q, Liu CA, Li S, Yan Y, Yu ST, Huang L. Micronized cellulose particles from mechanical treatment and their performance on reinforcing polypropylene composite. *Cellulose*. Jan 2023;30(1):235-246. doi:https://doi.org/10.1007/s10570-022-04905-y

15. Bettaieb F, Khiari R, Dufresne A, Mhenni MF, Belgacem MN. Mechanical and thermal properties of Posidonia oceanica cellulose nanocrystal reinforced polymer. *Carbohyd Polym*. Jun 5 2015;123:99-104. doi:https://doi.org/10.1016/j.carbpol.2015.01.026

16. Ng HM, Sin LT, Bee ST, Tee TT, Rahmat AR. Review of Nanocellulose Polymer Composite Characteristics and Challenges. *Polym-Plast Technol*. 2017;56(7):687-731. doi:https://doi.org/10.1080/03602559.2016.1233277

17. Miao CW, Hamad WY. Critical insights into the reinforcement potential of cellulose nanocrystals in polymer nanocomposites. *Curr Opin Solid St M*. Aug 2019;23(4)doi:https://doi.org/10.1016/j.cossms.2019.06.005

18. Hanid NA, Wahit MU, Guo QP, Mahmoodian S, Soheilmoghaddam M. Development of regenerated cellulose/halloysites nanocomposites via ionic liquids. *Carbohyd Polym*. Jan 2 2014;99:91-97. doi:https://doi.org/10.1016/j.carbpol.2013.07.080

19. Corder RD, Adhikari P, Burroughs MC, Rojas OJ, Khan SA. Cellulose nanocrystals for gelation and percolation-induced reinforcement of a photocurable poly(vinyl alcohol) derivative. *Soft Matter*. Sep 30 2020;16(37):8602-8611. doi:https://doi.org/10.1039/D0SM01376E

20. Jardin JM, Zhang Z, Hu G, Tam KC, Mekonnen TH. Reinforcement of rubber nanocomposite thin sheets by percolation of pristine cellulose nanocrystals. *Int J Biol Macromol*. Jun 1 2020;152:428-436. doi:https://doi.org/10.1016/j.ijbiomac.2020.02.303

21. Kim HJ, Choi YH, Jeong JH, et al. Rheological Percolation of Cellulose Nanocrystals in Biodegradable Poly(butylene succinate) Nanocomposites: A Novel Approach for Tailoring the Mechanical and Hydrolytic Properties. *Macromol Res*. Oct 2021;29(10):720-726. doi:https://doi.org/10.1007/s13233-021-9080-x

22. Santamaria-Echart A, Ugarte L, García-Astrain C, Arbelaiz A, Corcuera MA, Eceiza A. Cellulose nanocrystals reinforced environmentally-friendly waterborne polyurethane nanocomposites. *Carbohyd Polym*. Oct 20 2016;151:1203-1209. doi:https://doi.org/10.1016/j.carbpol.2016.06.069

23. Forsgren L, Venkatesh A, Rigoulet F, et al. Water-assisted extrusion and injection moulding of composites with surface-grafted cellulose nanocrystals - An upscaling study. *Compos Part B-Eng*. Mar 1 2021;208doi:https://doi.org/10.1016/j.compositesb.2020.108590

24. Samir MASA, Alloin F, Sanchez JY, Dufresne A. Cellulose nanocrystals reinforced poly(oxyethylene). *Polymer*. May 20 2004;45(12):4149-4157. doi:https://doi.org/10.1016/j.polymer.2004.03.094

25. Crank J. *The mathematics of diffusion*. Oxford university press; 1979.

26. Wang W, Sain M, Cooper PA. Study of moisture absorption in natural fiber plastic composites. *Compos Sci Technol*. Mar 2006;66(3-4):379-386. doi:https://doi.org/10.1016/j.compscitech.2005.07.027

27. Aumnate C, Rudolph N, Sarmadi M. Recycling of Polypropylene/Polyethylene Blends: Effect of Chain Structure on the Crystallization Behaviors. *Polymers-Basel*. Sep 2019;11(9)doi:https://doi.org/10.3390/polym11091456

28. Suzuki K, Sato A, Okumura H, Hashimoto T, Nakagaito AN, Yano H. Novel high-strength, micro fibrillated cellulose-reinforced polypropylene composites using a cationic polymer as compatibilizer. *Cellulose*. Feb 2014;21(1):507-518. doi:https://doi.org/10.1007/s10570-013-0143-9

29. Wang L, Roach AW, Gardner DJ, Han Y. Mechanisms contributing to mechanical property changes in composites of polypropylene reinforced with spray-dried cellulose nanofibrils. *Cellulose*. Jan 2018;25(1):439-448. doi:https://doi.org/10.1007/s10570-017-1556-7

30. de Carvalho MS, Azevedo JB, Barbosa JDV. Effect of the melt flow index of an HDPE matrix on the properties of composites with wood particles. *Polym Test*. Oct 2020;90doi:https://doi.org/10.1016/j.polymertesting.2020.106678

31. Bahar E, Ucar N, Onen A, et al. Thermal and mechanical properties of polypropylene nanocomposite materials reinforced with cellulose nano whiskers. *J Appl Polym Sci*. Aug 15 2012;125(4):2882-2889. doi: https://doi.org/10.1002/app.36445

32. Felix JM, Gatenholm P. The Nature of Adhesion in Composites of Modified Cellulose Fibers and Polypropylene. *J Appl Polym Sci*. Feb 5 1991;42(3):609-620. doi:https://doi.org/10.1002/app.1991.070420307

33. Ashori A, Sheshmani S. Hybrid composites made from recycled materials: Moisture absorption and thickness swelling behavior. *Bioresource Technol*. Jun 2010;101(12):4717-4720. doi:https://doi.org/10.1016/j.biortech.2010.01.060

34. Ng HM, Sin LT, Tee TT, et al. Extraction of cellulose nanocrystals from plant sources for application as reinforcing agent in polymers. *Compos Part B-Eng*. Jun 15 2015;75:176-200. doi:https://doi.org/10.1016/j.compositesb.2015.01.008

35. Gray DG. Transcrystallization of polypropylene at cellulose nanocrystal surfaces. *Cellulose*. Apr 2008;15(2):297-301. doi:https://doi.org/10.1007/s10570-007-9176-2

36. Quillin DT, Caulfield DF, Koutsky JA. Crystallinity in the Polypropylene/Cellulose System .1. Nucleation and Crystalline Morphology. *J Appl Polym Sci*. Nov 15 1993;50(7):1187-1194. doi:https://doi.org/10.1002/app.1993.070500709

37. Amash A, Zugenmaier P. Morphology and properties of isotropic and oriented samples of cellulose fibre-polypropylene composites. *Polymer*. Feb 2000;41(4):1589-1596. doi:https://doi.org/10.1016/S0032-3861(99)00273-6

38. Chen HB, Karger-Kocsis J, Wu JS, Varga J. Fracture toughness of α- and β-phase polypropylene homopolymers and random- and block-copolymers. *Polymer*. Nov 2002;43(24):6505-6514. doi:https://doi.org/10.1016/S0032-3861(02)00590-6

39. Wang XC, Song RF, Chen YJ, Zhao YH, Zhu KY, Yuan XY. Mechanical properties of polypropylene by diversely compatibilizing with titanate whiskers in composites. *Compos Sci Technol*. Aug 18 2018;164:103-109. doi:https://doi.org/10.1016/j.compscitech.2018.05.036

40. Li XX, Wu HY, Wang Y, Bai HW, Liu L, Huang T. Study on the β to α transformation of PP/POE blends with β-phase nucleating agent during the tensile deformation process. *Mat Sci Eng a-Struct*. Jan 15 2010;527(3):531-538. doi:https://doi.org/10.1016/j.msea.2009.08.007

41. Shirvanimoghaddam K, Balaji KV, Yadav R, et al. Balancing the toughness and strength in polypropylene composites. *Compos Part B-Eng*. Oct 15 2021;223doi:https://doi.org/10.1016/j.compositesb.2021.109121

Chapter 4 Conclusions and Future Research

4.1 Conclusions

The overall goal of this research is subdivided into two specific objectives: 1) develop composites with different loading levels of SDCNC particles and characterize the effect of loading levels of SDCNC on composite mechanical and thermal properties to identify the percolation threshold of the SDCNC particles in the HPP matrix and 2) understand the effect of the compatibilizer of MAPP on composite mechanical and thermal properties near the SDCNC percolation threshold.

The SDCNC particle-reinforced HPP composites were successfully manufactured with a masterbatch concept using a C.W. Brabender internal bowl mixer followed by an injection molding process. The effect of the SDCNC particles and their loading levels (5, 10, 15, and 30 wt.%) on the mechanical, morphological, and thermal properties of HPP composites was investigated. Compared to the neat HPP, the tensile and flexural MOE of composites were significantly improved by approximately 67% and 49%, and the impact strength was significantly increased by 19%. However, the tensile strength and strain at yield remarkably decreased because of the absence of any compatibilizer that can improve the compatibility and interfacial adhesion between the hydrophilic SDCNC particles and the hydrophobic HPP. The enhancement in impact strength was attributed to the establishment of mechanical interlocking between the SDCNC particles and the HPP matrix observed from the SEM. The crystallization peak temperature of CNC/HPP

composites increased with increasing SDCNC loading levels from the DSC measurement. The SDCNC particles can act as heterogeneous nucleating agents to promote the crystallization process of HPP. The observations from the TGA demonstrated a slight improvement in the thermal stability of HPP composites after introducing the SDCNC particles.

The HPP composites reinforced with varying loading levels of SDCNC at 20, 30, 40, and 50 wt. % were continuously prepared to identify the percolation threshold of SDCNC particles within the HPP matrix and to estimate the impact of this percolation threshold on the mechanical and thermal properties of the HPP composites. Water absorption testing was used as a novel tool to predict the percolation threshold of the SDCNC in the HPP matrix. Moreover, the effect of MAPP at the loading levels of 3, 5, and 7 wt. % on the percolation network and mechanical and thermal properties were studied. Compared to the neat HPP, the tensile and flexural MOE of the CNC/HPP composites were significantly increased by 123 % and 117 %. The SDCNC percolation threshold in HPP composites was estimated to be between 30 – 40 wt. % as there was a significant increment in flexural strength (4%) and impact strength (22%) when the SDCNC content reached 30 wt. %, followed by a subsequent decline in both 40 and 50 wt.% loadings, compared to neat HPP. The water gain and dimensional swell changed dramatically above 30 wt. % SDCNC, indicating a notable change in the internal structure of the SDCNC particles in the composites. The crystallization behaviors of the HPP were also altered with the presence of SDCNC with the loading up to 30 wt.%. The crystallization behavior changes of the composites diminished at 40 and 50 wt.% of SDCNC loadings, which are above the percolation threshold of the SDCNC

particle. At the percolation threshold, the SDCNC particles provided a saturated nucleation function, and higher loading level cannot change the nucleation function anymore. With the addition of MAPP, there was a minor influence on the internal structure of the SDCNC particles in the HPP matrix with the loading of 30 wt.% and a more considerable influence at 40 wt.% loading. A maximal enhancement in tensile strength (58%), tensile strain (61%), flexural strength (45%), and impact strength (91%) was observed compared to the corresponding composite without MAPP. These improvements were ascribed to the enhanced interfacial adhesion between the particles and the matrix from the SEM observation. However, MAPP altered the crystallization process of HPP in the CNC/MAPP/HPP composites compared to the CNC/HPP composites, which was likely caused by the diminished nucleation function of the SDCNC particles. The chemical reaction between MAPP and the SDCNC particles covered the surface, reducing the surface nucleation function and hindering the formation and growth of crystallite of HPP.

4.2 Future research

This thesis employed the SDCNC particles to strengthen the HPP properties using a melt compounding process coupled with an injection molding procedure. MAPP was used as a coupling agent to improve the compatibility between the particles and the matrix, thus enhancing the interfacial strength. It has been proved that MAPP can significantly improve the mechanical properties of the SDCNC HPP composites. However, the SEM images shown in Figure 3-1E-F seem to indicate that the CNC/MAPP/HPP composites fractured within the region of the MAPP

phase. That can be explained by the fact that the MAPP used has a very high MFI (115 g /10 min) and low molecular weight compared to the HPP matrix (20 g/10 min), meaning the MAPP polymer chain's strength and stability are the weak points. When MAPP was diffused inside the HPP matrix, the entanglement between them was weak and more susceptible to failure when subjected to external force, causing a suboptimal interfacial strength. [1] As discussed in Chapter 3, the interfacial adhesion between reinforcement and matrix plays a critical role in achieving satisfactory properties of composites. Therefore, the next step of the research is to optimize the SDCNC particles reinforced HPP composites by further improving the interfacial adhesion strength between SDCNC and HPP, such as studying the effect of the different types of MAPP with varying high molecular weights on the properties of the resulted composites to fabricate high-performance composites.

The crystallinity of semicrystalline polymer is a crucial factor in determining its performance. The SDCNC particles can serve as effective heterogeneous nucleating agents for the crystallization process of the HPP based on our DSC results. However, the addition of rigid particles can also restrict the polymer chain’s movement and thus influence the crystal growth. Therefore, it is essential to estimate the nucleation and crystal growth for optimizing the HPP composite properties. The effect of a low concentration of spray freeze-dried CNC (1 wt. %) on the isothermal crystallization kinetics of PP was investigated. [2] However, isothermal crystallization disregards the cooling rate and thermal gradient effect within the composites, which commonly occurs in the real production process. Non-isothermal crystallization is more commonly

encountered in practical industrial processing and thus can offer better information on the crystallization process. Hence, future work will be necessary to study the effect of different loading levels of the SDCNC particles on the non-isothermal crystallization kinetics of the HPP composites. The influence of MAPP on the crystallization rate of HPP composites near the SDCNC percolation threshold will also be an interest to be researched.

The water absorption results showed that the SDCNC particles as reinforcement in polymer composites behave better than other natural fibers when exposed to a wet environment for a long time because of the relatively lower water gain values. But the effect of water absorption on the mechanical properties of HPP composites is unknown, which is momentous in practical utilization. The study of the impact of water absorption on the mechanical properties of the SDCNC particle-reinforced HPP composite is worthy of exploration, especially near the SDCNC percolation threshold, where the SDCNC particles connect and form the continuous networks inside the composites.

4.3 References

1. Kim H-S, Lee B-H, Choi S-W, Kim S, Kim H-J. The effect of types of maleic anhydride-grafted polypropylene (MAPP) on the interfacial adhesion properties of bio-flour-filled polypropylene composites. *Composites Part A: Applied Science Manufacturing*. 2007;38(6):1473-1482.

2. Khoshkava V, Ghasemi H, Kamal MR. Effect of cellulose nanocrystals (CNC) on isothermal crystallization kinetics of polypropylene. Thermochimica Acta. 2015;608:30-39. doi:https://doi.org/10.1016/j.tca.2015.04.007

References

1. Hon DN-S. Cellulose: a random walk along its historical path. *Cellulose*. 1994;1(1):1-25.

2. Moon RJ, Martini A, Nairn J, Simonsen J, Youngblood J. Cellulose nanomaterials review: structure, properties and nanocomposites. *Chemical Society Reviews*. 2011;40(7):3941-3994.

3. Klemm D, Heublein B, Fink HP, Bohn A. Cellulose: fascinating biopolymer and sustainable raw material. *Angewandte chemie international edition*. 2005;44(22):3358-3393.

4. Dinand E, Vignon M, Chanzy H, Heux L. Mercerization of primary wall cellulose and its implication for the conversion of cellulose I→ cellulose II. *Cellulose*. 2002;9(1):7-18.

5. Roy D, Semsarilar M, Guthrie JT, Perrier S. Cellulose modification by polymer grafting: a review. *Chemical Society Reviews*. 2009;38(7):2046-2064.

6. Phanthong P, Reubroycharoen P, Hao X, Xu G, Abudula A, Guan G. Nanocellulose: Extraction and application. *Carbon Resources Conversion*. 2018;1(1):32-43.

7. Lucia LA, Rojas OJ. Fiber nanotechnology: a new platform for “green” research and technological innovations. *Cellulose*. 2007;14(6):539-542.

8. Moon RJ, Frihart CR, Wegner T. Nanotechnology applications in the forest products industry. *Forest products journal Vol 56, no 5 (May 2006): pages 4-10*. 2006;

9. Jasmani L, Rusli R, Khadiran T, Jalil R, Adnan S. Application of nanotechnology in wood-based products industry: A review. *Nanoscale research letters*. 2020;15(1):1-31.

10. Peng BL, Dhar N, Liu H, Tam K. Chemistry and applications of nanocrystalline cellulose and its derivatives: a nanotechnology perspective. *The Canadian journal of chemical engineering*. 2011;89(5):1191-1206.

11. Rajinipriya M, Nagalakshmaiah M, Robert M, Elkoun S. Importance of agricultural and industrial waste in the field of nanocellulose and recent industrial developments of wood based nanocellulose: a review. *ACS Sustainable Chemistry & Engineering*. 2018;6(3):2807-2828.

12. Li B, Xu W, Kronlund D, et al. Comparable characterization of nanocellulose extracted from bleached softwood and hardwood pulps. *Paper and Biomaterials*. 2018;3(4):35-44.

13. Bruce D, Hobson R, Farrent J, Hepworth D. High-performance composites from low-cost plant primary cell walls. *Composites Part A: Applied Science and Manufacturing*. 2005;36(11):1486-1493.

14. Morais JPS, de Freitas Rosa M, Nascimento LD, do Nascimento DM, Cassales AR. Extraction and characterization of nanocellulose structures from raw cotton linter. *Carbohydrate polymers*. 2013;91(1):229-235.

15. Dunlop MJ, Acharya B, Bissessur R. Isolation of nanocrystalline cellulose from tunicates. *Journal of Environmental Chemical Engineering*. 2018;6(4):4408-4412.

16. Dugan JM, Gough JE, Eichhorn SJ. Bacterial cellulose scaffolds and cellulose nanowhiskers for tissue engineering. *Nanomedicine*. 2013;8(2):287-298.

17. Hubbe MA, Rojas OJ, Lucia LA, Sain M. Cellulosic nanocomposites: a review. *BioResources*. 2008;3(3):929-980.

18. Klemm D, Kramer F, Moritz S, et al. Nanocelluloses: a new family of nature-based materials. *Angewandte Chemie International Edition*. 2011;50(24):5438-5466.

19. Lu Z, Fan L, Zheng H, Lu Q, Liao Y, Huang B. Preparation, characterization and optimization of nanocellulose whiskers by simultaneously ultrasonic wave and microwave assisted. *Bioresource technology*. 2013;146:82-88.

20. Naz S, Ali JS, Zia M. Nanocellulose isolation characterization and applications: a journey from non-remedial to biomedical claims. *Bio-Design and Manufacturing*. 2019;2(3):187-212.

21. Dufresne A. *Nanocellulose: from nature to high performance tailored materials*. Walter de Gruyter GmbH & Co KG; 2017.

22. Phisalaphong M, Jatupaiboon N. Biosynthesis and characterization of bacteria cellulose–chitosan film. *Carbohydrate Polymers*. 2008;74(3):482-488.

23. Hao W, Wang M, Zhou F, et al. A review on nanocellulose as a lightweight filler of polyolefin composites. *Carbohydr Polym*. Sep 1 2020;243:116466. doi:10.1016/j.carbpol.2020.116466

24. Hashaikeh R, Krishnamachari P, Samad YA. Nanomanifestations of Cellulose: Applications for Biodegradable Composites. *Handbook of Polymer Nanocomposites Processing, Performance and Application*. 2015:229-248:chap Chapter 60.

25. Khan A, Huq T, Khan RA, Riedl B, Lacroix M. Nanocellulose-based composites and bioactive agents for food packaging. *Critical reviews in food science and nutrition*. 2014;54(2):163-174.

26. Dufresne A. Nanocellulose Processing Properties and Potential Applications. *Current Forestry Reports*. 2019;5(2):76-89. doi:10.1007/s40725-019-00088-1

27. Dufresne A. Nanocellulose: potential reinforcement in composites. *Natural polymers*. 2012;2:1-32.

28. Tashiro K, Kobayashi M. Theoretical evaluation of three-dimensional elastic constants of native and regenerated celluloses: role of hydrogen bonds. *Polymer*. 1991;32(8):1516-1526.

29. Quesada Cabrera Rl, Meersman F, McMillan PF, Dmitriev V. Nanomechanical and structural properties of native cellulose under compressive stress. *Biomacromolecules*. 2011;12(6):2178-2183.

30. Omran AAB, Mohammed AA, Sapuan S, et al. Micro-and nanocellulose in polymer composite materials: A review. *Polymers*. 2021;13(2):231.

31. Karimian A, Parsian H, Majidinia M, et al. Nanocrystalline cellulose: Preparation, physicochemical properties, and applications in drug delivery systems. *International journal of biological macromolecules*. 2019;133:850-859.

32. Lin N, Dufresne A. Nanocellulose in biomedicine: Current status and future prospect. *European Polymer Journal*. 2014;59:302-325.

33. Ferreira FV, Pinheiro IF, de Souza SF, Mei LH, Lona LM. Polymer composites reinforced with natural fibers and nanocellulose in the automotive industry: A short review. *Journal of Composites Science*. 2019;3(2):51.

34. Li F, Biagioni P, Bollani M, Maccagnan A, Piergiovanni L. Multi-functional coating of cellulose nanocrystals for flexible packaging applications. *Cellulose*. 2013;20(5):2491-2504.

35. Vineeth S, Gadhave RV, Gadekar PT. Nanocellulose applications in wood adhesives. *Open Journal of Polymer Chemistry*. 2019;9(4):63-75.

36. Boldizar A, Klason C, Kubat J, Näslund P, Saha P. Prehydrolyzed cellulose as reinforcing filler for thermoplastics. *International Journal of Polymeric Materials*. 1987;11(4):229-262.

37. Kargarzadeh H, Mariano M, Huang J, et al. Recent developments on nanocellulose reinforced polymer nanocomposites: A review. *Polymer*. 2017;132:368-393. doi:https://doi.org/10.1016/j.polymer.2017.09.043

38. Lee K-Y, Aitomäki Y, Berglund LA, Oksman K, Bismarck A. On the use of nanocellulose as reinforcement in polymer matrix composites. *Composites Science and Technology*. 2014;105:15-27.

39. Börjesson M, Westman G. Crystalline nanocellulose—preparation, modification, and properties. *Cellulose-fundamental aspects and current trends*. 2015;7

40. Bledzki A, Gassan J. Composites reinforced with cellulose based fibres. *Progress in polymer science*. 1999;24(2):221-274.

41. Lotfi A, Li H, Dao DV, Prusty G. Natural fiber–reinforced composites: A review on material, manufacturing, and machinability. *Journal of Thermoplastic Composite Materials*. 2021;34(2):238-284.

42. Yu M-F, Lourie O, Dyer MJ, Moloni K, Kelly TF, Ruoff RS. Strength and breaking mechanism of multiwalled carbon nanotubes under tensile load. *Science*. 2000;287(5453):637-640.

43. Carpenter AW, de Lannoy C-F, Wiesner MR. Cellulose nanomaterials in water treatment technologies. *Environmental science & technology*. 2015;49(9):5277-5287.

44. Yang X, Han F, Xu C, et al. Effects of preparation methods on the morphology and properties of nanocellulose (NC) extracted from corn husk. *Industrial Crops and Products*. 2017;109:241-247.

45. Liu H, Liu D, Yao F, Wu Q. Fabrication and properties of transparent polymethylmethacrylate/cellulose nanocrystals composites. *Bioresource technology*. 2010;101(14):5685-5692.

46. Lu H, Gui Y, Zheng L, Liu XJFRI. Morphological, crystalline, thermal and physicochemical properties of cellulose nanocrystals obtained from sweet potato residue. 2013;50(1):121-128.

47. Ng HM, Sin LT, Bee ST, Tee TT, Rahmat A. Review of nanocellulose polymer composite characteristics and challenges. *Polymer-Plastics Technology and Engineering*. 2017;56(7):687-731.

48. Bras J, Viet D, Bruzzese C, Dufresne A. Correlation between stiffness of sheets prepared from cellulose whiskers and nanoparticles dimensions. *Carbohydrate Polymers*. 2011;84(1):211-215.

49. Chen Y, Gan L, Huang J, Dufresne A. Reinforcing mechanism of cellulose nanocrystals in nanocomposites. *Nanocellulose: from fundamentals to advanced materials*. 2019:201-249. doi: https://doi.org/10.1002/9783527807437.ch7

50. Favier V, Chanzy H, Cavaille J. Polymer nanocomposites reinforced by cellulose whiskers. *Macromolecules*. 1995;28(18):6365-6367.

51. Dufresne A. Nanocellulose: a new ageless bionanomaterial. *Materials today*. 2013;16(6):220-227. doi:https://doi.org/10.1016/j.mattod.2013.06.004

52. Mariano M, Dufresne A. Nanocellulose: common strategies for processing of nanocomposites. *Nanocelluloses: Their Preparation, Properties, and Applications*. ACS Publications; 2017:203-225.

53. Khoshkava V, Kamal MR. Effect of cellulose nanocrystals (CNC) particle morphology on dispersion and rheological and mechanical properties of polypropylene/CNC nanocomposites. *ACS applied materials & interfaces*. 2014;6(11):8146-8157.

54. Sojoudiasli H, Heuzey MC, Carreau PJ. Mechanical and morphological properties of cellulose nanocrystal-polypropylene composites. *Polymer Composites*. 2018;39(10):3605-3617. doi:https://doi.org/10.1002/pc.24383

55. Gray N, Hamzeh Y, Kaboorani A, Abdulkhani A. Influence of cellulose nanocrystal on strength and properties of low density polyethylene and thermoplastic starch composites. *Industrial Crops and Products*. 2018;115:298-305.

56. Oksman K, Mathew AP, Bondeson D, Kvien I. Manufacturing process of cellulose whiskers/polylactic acid nanocomposites. *Composites science and technology*. 2006;66(15):2776-2784.

57. Roman M, Winter WT. Effect of sulfate groups from sulfuric acid hydrolysis on the thermal degradation behavior of bacterial cellulose. *Biomacromolecules*. 2004;5(5):1671-1677. doi:https://doi.org/10.1021/bm034519+

58. Maddah HA. Polypropylene as a promising plastic: A review. *Am J Polym Sci*. 2016;6(1):1-11.

59. Yang HS, Gardner DJ, Nader JW. Characteristic impact resistance model analysis of cellulose nanofibril-filled polypropylene composites. *Composites Part A: Applied Science and Manufacturing*. 2011;42(12):2028-2035.

60. Sinquefield S, Ciesielski PN, Li K, Gardner DJ, Ozcan S. Nanocellulose dewatering and drying: current state and future perspectives. *ACS Sustainable Chemistry & Engineering*. 2020;8(26):9601-9615.

61. Peng Y, Gardner DJ, Han Y. Drying cellulose nanofibrils: in search of a suitable method. *Cellulose*. 2012a;19(1):91-102.

62. Bahar E, Ucar N, Onen A, et al. Thermal and mechanical properties of polypropylene nanocomposite materials reinforced with cellulose nano whiskers. *Journal of Applied Polymer Science*. 2012;125(4):2882-2889. doi:https://doi.org/10.1002/app.36445

63. Ljungberg N, Bonini C, Bortolussi F, Boisson C, Heux L, Cavaillé J-Y. New nanocomposite materials reinforced with cellulose whiskers in atactic polypropylene: effect of surface and dispersion characteristics. *Biomacromolecules*. 2005;6(5):2732-2739. doi:https://doi.org/10.1021/bm050222v

64. Sapkota J, Natterodt JC, Shirole A, Foster EJ, Weder C. Fabrication and properties of polyethylene/cellulose nanocrystal composites. *Macromolecular Materials and Engineering*. 2017;302(1):1600300.

65. Huan S, Bai L, Liu G, Cheng W, Han G. Electrospun nanofibrous composites of polystyrene and cellulose nanocrystals: manufacture and characterization. *Rsc Advances*. 2015;5(63):50756-50766.

66. Pei A, Zhou Q, Berglund LA. Functionalized cellulose nanocrystals as biobased nucleation agents in poly (l-lactide)(PLLA)–Crystallization and mechanical property effects. *Composites Science and Technology*. 2010;70(5):815-821.

67. Shrestha S, Montes F, Schueneman GT, Snyder JF, Youngblood JP. Effects of aspect ratio and crystal orientation of cellulose nanocrystals on properties of poly (vinyl alcohol) composite fibers. *Composites Science and Technology*. 2018;167:482-488.

68. Peresin MS, Vesterinen AH, Habibi Y, et al. Crosslinked PVA nanofibers reinforced with cellulose nanocrystals: Water interactions and thermomechanical properties. *Journal of Applied Polymer Science*. 2014;131(11)

69. Kumar A, Negi YS, Choudhary V, Bhardwaj NK. Morphological and Mechanical Properties of Cellulose Nanocrystals Reinforced Poly (vinyl alcohol) Bio-composite Films. *Trends in Carbohydrate Research*. 2015;7(2)

70. Trache D, Tarchoun AF, Derradji M, et al. Nanocellulose: From Fundamentals to Advanced Applications. *Front Chem*. 2020;8:392. doi:10.3389/fchem.2020.00392

71. Peng Y, Han Y, Gardner DJ. Spray-drying cellulose nanofibrils: Effect of drying process parameters on particle morphology and size distribution. *Wood and Fiber Science*. 2012b:448-461.

72. Kazayawoko M, Balatinecz J, Matuana L. Surface modification and adhesion mechanisms in woodfiber-polypropylene composites. *Journal of materials science*. 1999;34(24):6189-6199.

73. Zhou Y, Fan M, Chen L. Interface and bonding mechanisms of plant fibre composites: An overview. *Composites Part B: Engineering*. 2016;101:31-45.

74. Younas M, Noreen A, Sharif A, et al. A review on versatile applications of blends and composites of CNC with natural and synthetic polymers with mathematical modeling. *International journal of biological macromolecules*. 2019;124:591-626.

75. Islam MT, Alam MM, Zoccola M. Review on modification of nanocellulose for application in composites. *Int J Innov Res Sci Eng Technol*. 2013;2(10):5444-5451.

76. Peng Y, Gallegos SA, Gardner DJ, Han Y, Cai Z. Maleic anhydride polypropylene modified cellulose nanofibril polypropylene nanocomposites with enhanced impact strength. *Polymer composites*. 2016;37(3):782-793. doi:https://doi.org/10.1002/pc.23235

77. Techawinyutham L, Frick A, Siengchin S. Polypropylene/maleic anhydride grafted polypropylene (MAgPP)/coconut fiber composites. *Advances in Mechanical Engineering*. 2016;8(5):1687814016645446.

78. Yakkan E, Uysalman T, Atagür M, Sever K, Seydibeyoğlu MÖ. Nanocellulose-polypropylene nanocomposites enhanced with coupling agent. *Bartın Orman Fakültesi Dergisi*. 2018;20(3):491-502.

79. Qiu W, Zhang F, Endo T, Hirotsu T. Effect of maleated polypropylene on the performance of polypropylene/cellulose composite. *Polymer Composites*. 2005;26(4):448-453.

80. Qiu W, Endo T, Hirotsu T. Structure and properties of composites of highly crystalline cellulose with polypropylene: Effects of polypropylene molecular weight. *European Polymer Journal*. 2006;42(5):1059-1068.

81. Hassanabadi HM, Alemdar A, Rodrigue D. Polypropylene reinforced with nanocrystalline cellulose: Coupling agent optimization. *Journal of Applied Polymer Science*. 2015;132(34)

82. Suzuki K, Okumura H, Kitagawa K, Sato S, Nakagaito AN, Yano H. Development of continuous process enabling nanofibrillation of pulp and melt compounding. *Cellulose*. 2013;20(1):201-210.